submitted to **Journal of Space Weather and Space Climate**

Swarm Absolute Scalar Magnetometer Burst Mode: Observed ELF Signals and their Origins

A.J. Emsley[1,3], C.D. Beggan[1], A. Callow[2], K.A. Whaler[3], P. Coïsson[4], L. Chauvet[4], G. Hulot[4], and M. Jenner[4]

[1] British Geological Survey, Research Avenue South, Riccarton, Scotland, United Kingdom (e-mail: adam.emsley@bgs.ac.uk),
[2] School of Physics and Astronomy, University of Edinburgh, Scotland, United Kingdom,
[3] School of GeoSciences, University of Edinburgh, Scotland, United Kingdom,
[4] Université Paris Cité, Institut de physique du globe de Paris, CNRS, F-75005, France

ABSTRACT

The Absolute Scalar Magnetometers (ASM) onboard each European Space Agency Swarm satellites nominally provide 1 Hz magnetic scalar data. An additional experimental mode is available on the ASM consisting of a 250 Hz burst-mode which is periodically switched on allowing magnetic signals with frequencies up to 125 Hz to be investigated. By analysing burst-mode data from 2014 to 2023 in the frequency-time domain, we find a range of signals both man-made and geophysical, which we present here. Known features include lightning whistlers, auroral hiss and plasma bubbles that produce broadband incoherent signatures, and powerline harmonic radiation observed as stable 50 or 60 Hz lines. Ground based extremely low frequency (ELF) communication systems are also detected in the data. However, many as yet unexplained signals are observed. Rising-tone 70-125 Hz high-intensity bursts, lasting ~3 minutes, are found over the Antarctic, which we suggest are associated with local He^+ ion gyrofrequencies and thus are possibly narrow-banded ionospheric hiss. These signals appear to be associated with the South Atlantic Anomaly due to their clustering on its southern edge, with the low field strength producing He^+ gyrofrequencies less than 125 Hz. Additionally, extremely weak linear and quadratic chirps lasting tens of seconds to tens of minutes occur in the data without an obvious temporal or spatial trend which we tentatively attribute to onboard electronic or instrumental noise. Their origin requires further investigation to avoid artefacts in future magnetic missions. We also find long lasting, high frequency narrow-band features around 80-125 Hz which persist for 60-300 seconds, occurring orbit-on-orbit at fixed magnetic local times (MLT) around 0900 and 1500, mainly in equatorial latitudes, which are encountered during all burst sessions spanning these MLTs. The Swarm ASM burst-mode data suggest there are new geophysical magnetic phenomena yet to be fully understood, potentially offering new insights into magnetospheric and ionospheric wave-plasma interactions.

Key words. ELF magnetic field – Swarm satellite – ionosphere

This provisional PDF is the accepted version. The article should be cited as: J. Space Weather Space Clim., doi: 10.1051/swsc/2025028

1. Introduction

Earth's geomagnetic field interacts with the ionosphere, a conductive plasma layer extending approximately 80–600 km above the surface. This interaction is primarily driven by solar radiation, which induces complex electrical currents and wave phenomena. The magnetosphere above plays an important role in guiding and modulating waves within the ionosphere and serves as a source of waves and particles via the radiation belts. Studying electromagnetic signals in this region offers valuable insights into geophysical processes, including wave-particle interactions, ionospheric currents, and magnetosphere-ionosphere coupling. The Swarm mission was developed by the European Space Agency (ESA) with the aim of mapping the geomagnetic field to the highest possible level of accuracy (Friis-Christensen et al., 2006), and saw the successful launch of three identical satellites, Swarm A (Alpha), B (Bravo) and C (Charlie), in November 2013. For a short period of time after launch, Bravo and Charlie were kept on parallel orbits while the orbit of Alpha was lowered. Subsequently, the orbit of Bravo was raised and that of Charlie lowered to the altitude of Alpha. Since then Alpha and Charlie orbit in parallel, initially at around 475 km altitude, gradually reducing to 435 km over 8 years and subsequently having been raised to ~485 km in 2022 and further to ~495 km in 2023. Bravo orbits in a different plane at a higher, relatively consistent altitude of ~505-520 km (Fig. 1). Amongst the payloads on-board each craft are two identical high precision Absolute Scalar Magnetometers (ASM) (Léger et al., 2009). These instruments - one of which is included as a redundant backup - are placed at the end of the 4 m boom attached to each craft, minimising interference from the satellite electronics in the main housing. In nominal flight configuration, the ASM is at the rearmost point of the craft.

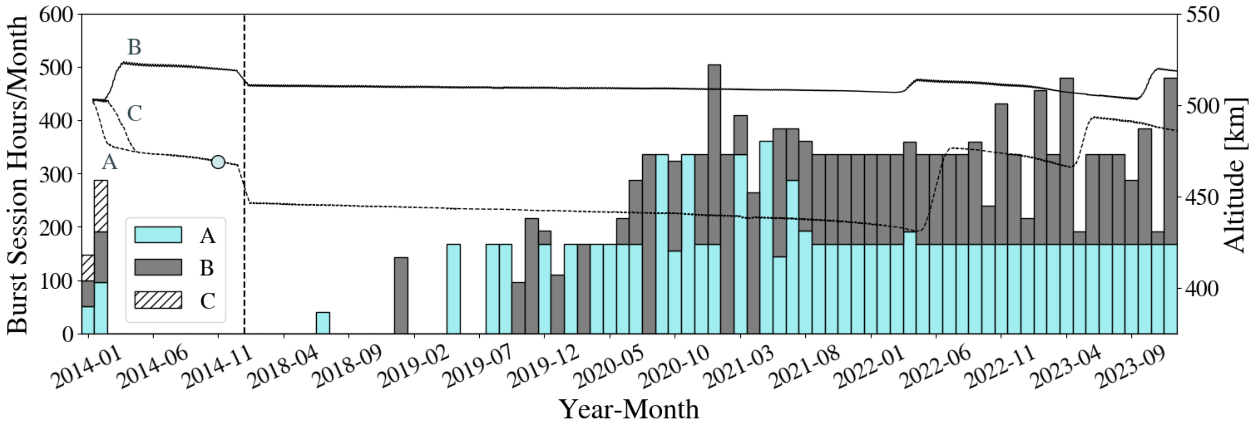

Fig. 1. Distribution of burst-mode data hours per month for 2014 and 2018 to 2023. The rolling 28-day mean altitude of each craft for this period is shown by the solid line for Swarm Bravo (B) and the dashed converging lines for Alpha (A) and Charlie (C). The open circle at 05-Nov-2014 indicates when Swarm Charlie stopped producing ASM data and the dashed vertical line indicates a break in the data from 2015 to 2017.

Scalar magnetic field data are provided by the ASM at a 1 Hz sampling rate for the Swarm Level1b product MAGX_LR_1B (Nielsen, 2021), downsampled from 50 Hz measurements; however the ASM sensors are also capable of running in a unique experimental 250 Hz "burst-mode" (Fratter et al., 2016). This then further allows magnetic signals in the band DC to 125 Hz to be detected. Measurements are made using atomic spectroscopy of ^{4}He, relying on optical pumping and radio-frequency driven resonance between Zeeman atomic sublevels, and have a resolution independent of the ambient field of around 1 pT/$\sqrt{\text{Hz}}$ (Léger et al., 2015). This burst-mode is run whenever the ASM are not run in another experimental "vector" mode using three orthogonal coils to perturb the scalar field in a controlled way to generate a 1 Hz high-quality self-calibrated vector measurement (Léger et al., 2009), as demonstrated in the context of global field modeling (Hulot et al., 2015; Vigneron et al., 2015, 2021). The operation of the optical pumping laser and of the radio-frequency modulation produce known modulations around 3 and 29 Hz (Fratter et al., 2016).

In total there have been 109 burst-mode sessions, generally lasting 7 days, with 14 shorter one to two days sessions, across all three craft in the period 2014-2023. The first burst sessions in early 2014 were run simultaneously on each satellite for short periods (usually less than one day) during the calibration and validation phase of the mission. Following the unfortunate failure of both ASM sensors on-board Swarm Charlie, the first at launch, the second on 05-Nov-2014, no more burst sessions could later be run on Charlie. Despite the limited availability of data, analysis of the 250 Hz data from the earliest sessions revealed the presence of lightning-generated electromagnetic whistlers with durations of 1–2 seconds (Coïsson et al., 2016).

Burst-mode was restarted in 2018 with regular sessions resuming in 2019, running alternately on Swarm Alpha and Bravo approximately one week at a time, twice per month (Coïsson et al., 2021) with the aim of covering all local times and seasons and solar cycle phases as evenly as possible during subsequent data collection. The burst sessions are not necessarily collected simultaneously on both satellites, though this occasionally happened in 2022, for example. Figure 1 shows the number of hours of data collected each month from 2014 to the end of 2023.

In this study, we do not discuss short-lasting signals such as whistlers, a first investigation of which has recently been reported by Jenner et al. (2024). Rather, we focus on the plethora of longer duration signals - those lasting one to tens of minutes that can be found in the burst-mode data. We provide an overview of their characteristics and behaviour and whether their source can be confidently identified or not. We first describe the methodology for processing the voluminous ASM burst-mode data, followed by an overview of known signals. We then examine signals that, as yet, have no confirmed source. This study is the first in-depth analysis of such longer lasting signals. Swarm burst-mode data reveal that there are mechanisms within the ionosphere that are yet to be understood. We aim to provide a brief overview of their occurrences and propose their origins where appropriate.

2. Methodology

Burst-mode data for the three satellites are analysed from all sessions spanning 2014 to 2023. We use version 0302 of the data, released between February and December 2023. The burst-mode data are experimental, and various known instrumental effects impact the data, including the sensor heater, motor and harmonics of the laser-system induced resonances (Léger et al., 2015). However, they have been meticulously examined and corrected for other issues such as bit-overflows and non-uniform time sampling (Chauvet and Hulot, 2023). Despite this, there remain relatively large spikes, typically flagged in the product, which must be removed for signal analysis. To achieve this consistently, the CHAOS-7.17 geomagnetic model (Finlay et al., 2020) with the static lithospheric field, as well as the time-dependent core and near-magnetospheric fields, was subtracted to obtain the total field residuals (F_R). To find and remove data spikes, the residuals were detrended by applying a Gaussian convolution filter with a standard deviation of 10 nT to F_R. This produced the long wavelength component of the residual, which was subtracted from F_R, giving F_D, and effectively acts as a high-pass filter, detrended the signal. Spikes in the data then become obvious and the median absolute deviation (MAD) approach is used to remove them. With 10-second time windows (equation 1), the outliers can be found and successfully removed by setting a threshold of $\alpha = 6$:

$$\frac{|x_i - \text{median}\,(x)\,|}{\text{median}\,(|x - \text{median}\,(x)\,|)} > \alpha \tag{1}$$

where x_i is deemed an outlier, in a window of data x, if the threshold α is exceeded. Outliers in F_R were replaced by the filtered (smoothed) residual used for detrending. Spectral analysis shows that the smoothed residual has little high frequency power and does not introduce additional artefacts into the magnetic time-series. Around 0.5% of the values are removed using this filter, which equates to 5-10 times the number of flagged outliers in a typical day of data. Outliers act as pseudo-impulsive signals which manifest as narrow high-power broadband artefacts in spectrograms; using the MAD technique was found to be visually adequate in order to alleviate these effects.

The residuals are then visualised as spectrograms for frequencies above 15 Hz. Below 15 Hz the energy from other low frequency ionospheric and/or magnetospheric sources exceeds the magnitude of signals of interest. After experimentation with the time/frequency trade off, we generated spectrograms using 132-sample windows (approximately 0.53 seconds), using an overlap between consecutive windows of 131. We then apply a Short-Time Fourier Transform (STFT) of length 256 (via zero-padding) to analyse the frequency content. The choice of these parameters was made through trial-and-error and assessed as appropriate by inspection of known effects like powerline harmonic radiation, whistlers and plasma bubbles. This gives a frequency resolution of ~1 Hz and thus a temporal resolution of ~1/250 s. The work flow is illustrated in Figure 2.

3. Analysis and Results

We use a number of other Swarm data products to better understand the possible sources of the high frequency signals visible in the spectrograms. Swarm Level1b plasma density measurements, derived from the Langmuir probes on each craft (Knudsen et al., 2017) and Level2 field aligned current (FAC), auroral oval boundary (AOB) (Ritter et al., 2013) and ionospheric bubble index (IBI) products (Park et al., 2013) are used to check correlations between signals and geophysical mechanisms. These datasets are accessible through the VirESclient module in Python (Smith et al., 2022) and allow us to produce a set of information-dense plots (see Figure 3 for detailed explanation) to cross-compare data from different sensors and processing chains. All signals were visually identified initially by inspection from the spectrograms with further analysis carried out for this introductory study on a small number described below.

The spectrogram in Figure 3 and subsequent figures shows the frequency from 15 Hz to 125 Hz (left axis) against time with the logarithm of spectral energy shown by colour. The colour scale runs from light blue (lowest spectral power) to orange and red (most powerful), with the energy scale set to enhance the contrast of the weaker signals against the background. The time axis denotes both Magnetic Local Time (upper labels) and Universal Time (UTC) (lower labels, in square brackets).

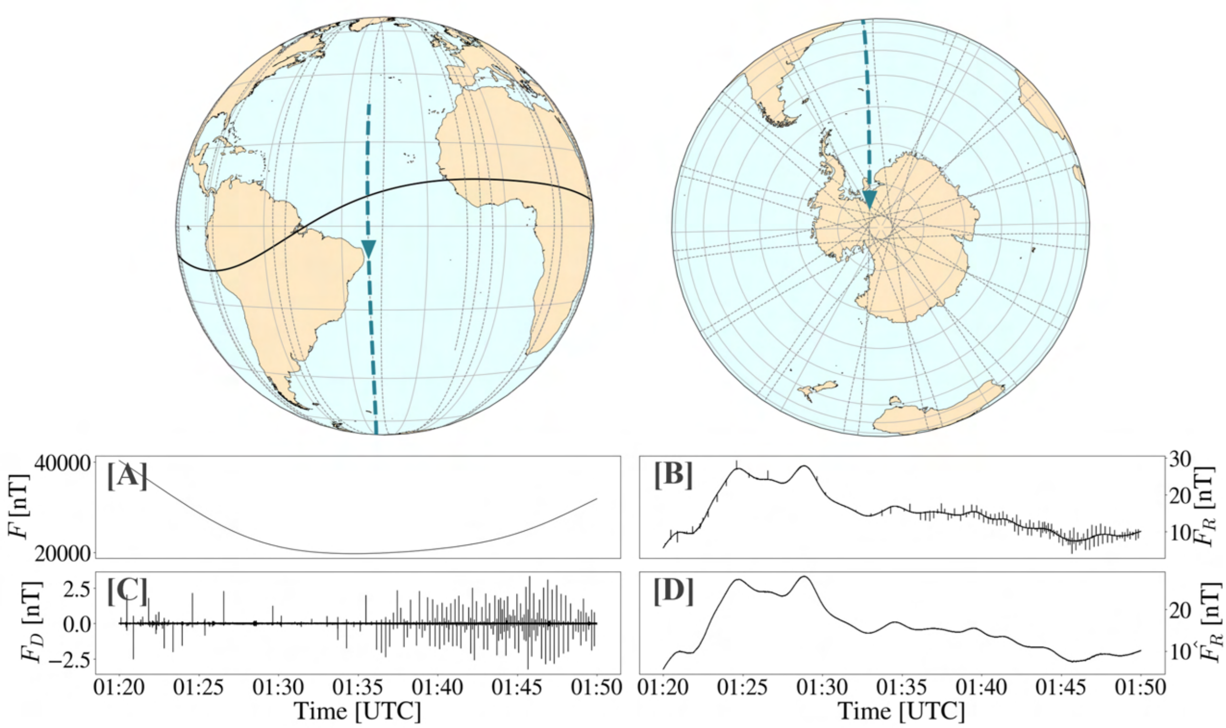

Fig. 2. Data processing chain for 30 minutes of Swarm Alpha burst-mode data collected along the thick blue dashed line on 16-Feb-2022. Grey dashed lines show the orbit of the entire day of burst-mode data, and the solid black line is the magnetic dip equator, calculated using the CHAOS-7.17 model at 500 km altitude. The field residual [B] is obtained from the raw signal [A] by subtracting the total field (F) component of the CHAOS-7.17 model. The signal is detrended via subtraction of the residual after applying a Gaussian convolution (σ = 10) filter [C] to better identify outliers. Outliers are then replaced by the filtered (smoothed) residual [D] and the signal is then ready for spectral analysis.

We first describe signals whose sources are known and well understood, followed by signals whose source is not known.

3.1. Powerline Harmonic Radiation and ELF Communication

The top panel in Figure 4 shows a spectrogram for Swarm Alpha for 18 minutes (00:25 to 00:43 UT) of an orbit on 17-Jan-2023 during low geomagnetic activity (Kp = 0). Several higher intensity signals are visible. Firstly a persistent spectral line occurs at ~29 Hz in all the data. This is related to a known aliasing of the radio frequency modulation driving the sensor (Léger et al., 2015). In this particular spectrogram example, two common manmade signals are highlighted (black boxes). Powerline harmonic radiation (PLHR) is often found to leak into the ionosphere and can be observed in the burst-mode data. PLHR is predominantly visible in spectrograms during nightside orbits, which can be attributed to shielding of the atmosphere during the day where ionospheric conditions such as plasma density are enhanced, and wave attenuation is greater. Dayside PLHR

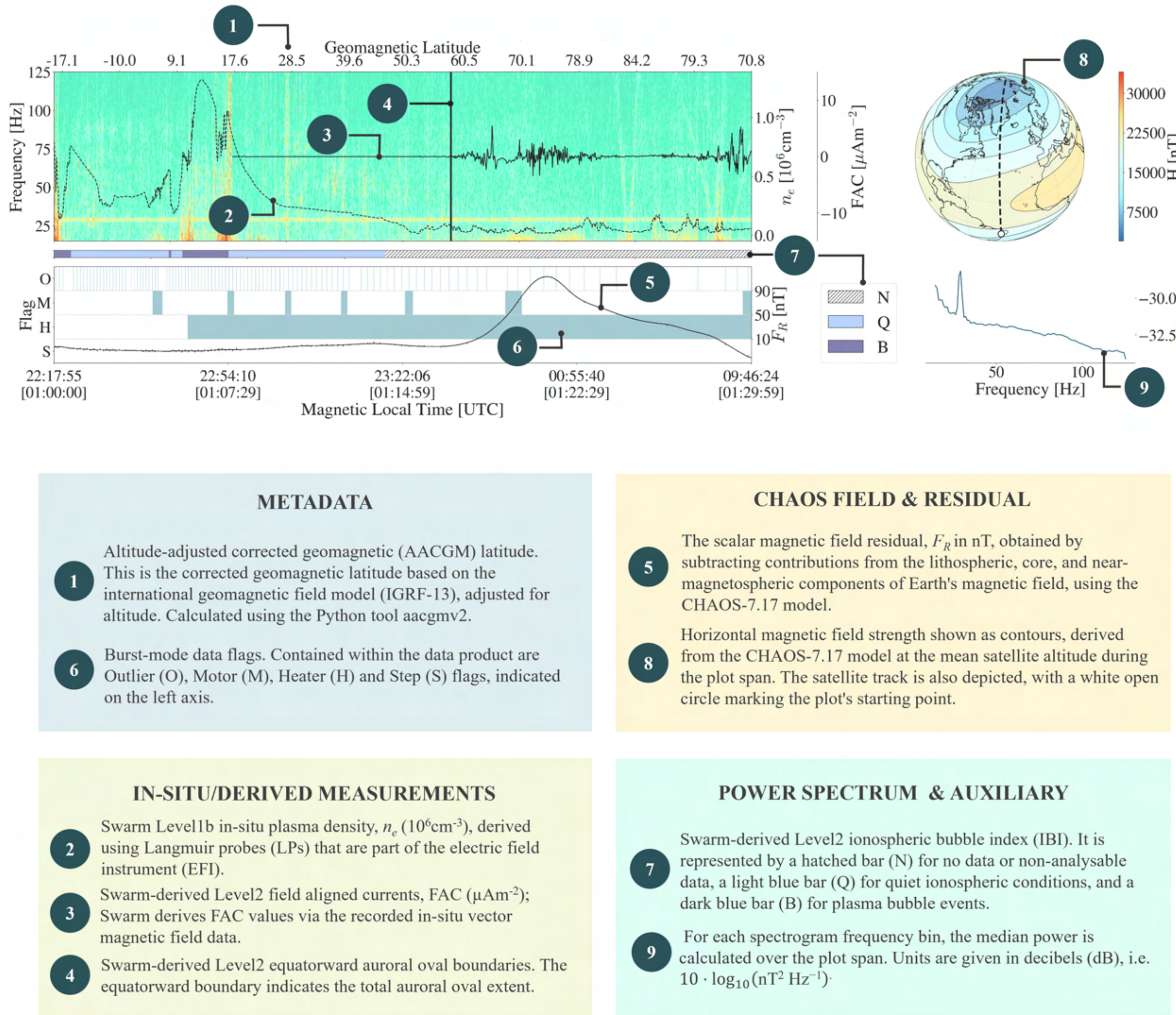

Fig. 3. Example spectrogram with legend describing the panels and data used for analysis, generated from Swarm Bravo data on 04-Nov-2022 from UTC 01:00 to UTC 01:30, with additional datasets for interpretation as labelled.

event detection following the method of Zhao et al. (2022) is found to occur but less frequently than during nightside. Depending on the region both 50 Hz and 60 Hz spectral lines can be detected as shown by DEMETER (Němec et al., 2015; Dudkin et al., 2015). We also observe instabilities in the base frequency, with shifts of ±0.1 Hz seen over India for example. PLHR is detected not only while the satellite footprint is over land but is noted to persist off the east coast of North/Central America and over the Indian Ocean on multiple occasions, hundreds of kilometres from the source. Additionally, at higher frequencies, extremely low frequency (ELF) communication signals are also visible in some areas of the world and even during dayside transit. The ZEVS ELF transmitter in western Russia (Pilipenko et al., 2019) is seen particularly well up to 1000 km from the source, as shown in Figure 4. Other ELF signals can be observed over China at ~90 Hz (not shown in Figure 4), for example.

PLHR detection rates derived in 10 second data windows with all burst-mode data available in 2020 to 2022 are geographically mapped in Figure 4 at 50 Hz and 60 Hz, binning data to a spatial resolution of 2.5°×2.5° and demonstrating similar results to those produced using the China Seismo-Electromagnetic Satellite (CSES) electric field sensor as mapped by Liao et al. (2024). We additionally plot ZEVS detection events at 82 Hz, binning to a resolution of 1°×1°. Event detection is computed as the percentage of events detected in a spatial bin with respect to the total number of time windows within the bin. In Figure 4, the peak spectral density power for the 29 Hz interference (denoted by 'I'), 50 Hz PLHR and ZEVS transmitter are 6.30 pT/Hz^2, 3.33 pT/Hz^2 and 4.37 pT/Hz^2, respectively.

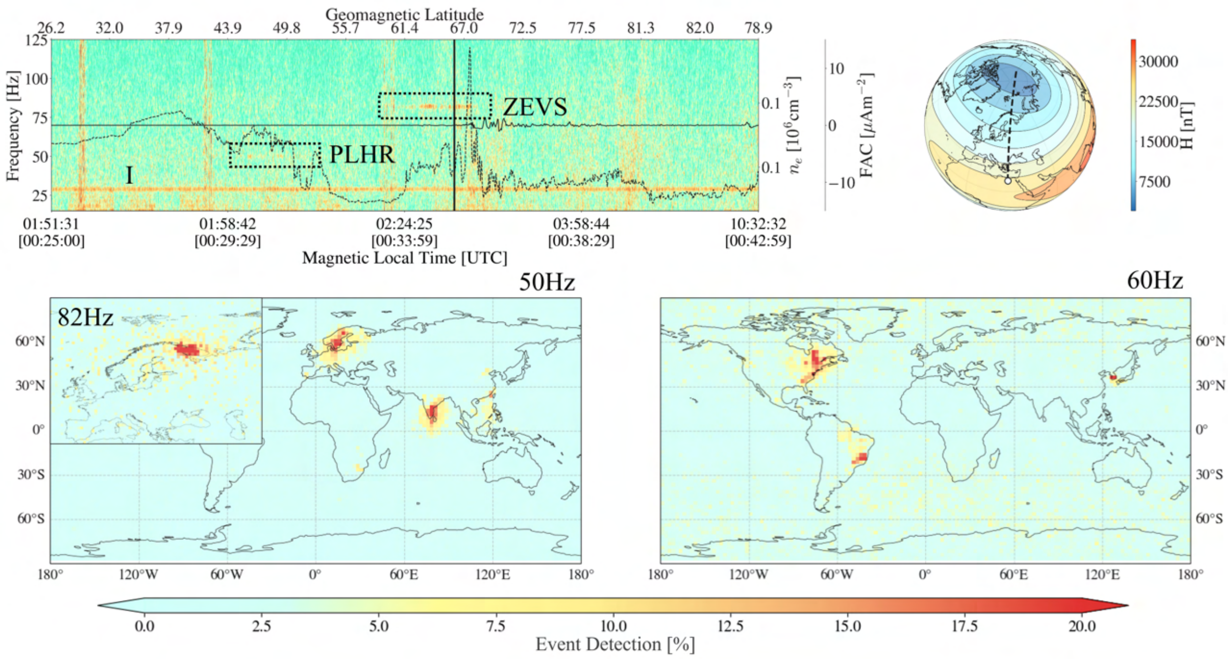

Fig. 4. Top: Spectrogram of Swarm Alpha data on 17-Jan-2023 from UTC 00:25:00-00:43:00 on a quiet day (Kp=0) illustrating 50 Hz powerline harmonic radiation (PLHR) and the 82 Hz signal produced by the Russian ZEVS transmitter. See Figure 3 for further details. Bottom: Distribution of ZEVS event detection (82 Hz) [inset] and PLHR events at 50 Hz (left) and 60 Hz (right) using all available 2020 to 2022 burst-mode data for Swarm Alpha and Bravo in 10 second windows.

3.2. Auroral Hiss and Plasma Bubbles

Signatures resembling auroral hiss (e.g. Santolík et al., 2006) are observed as semi-structured incoherent signals in the data (Fig. 5), though are relatively uncommon, often only being seen for 1-2 of the ~32 polar crossings each day for a given satellite. On some exceptional days, over 50% of polar crossings demonstrate clear examples. It is found to manifest during strong perturbations in the FAC measurements, as well as being attenuated during large drops in Swarm measurements of the in-situ plasma density. Occurrences of auroral hiss are approximately twice as common and often more intense over the southern auroral zone compared to the northern hemisphere, although a more thorough statistical review is needed. Plasma density irregularities are seen to coexist with auroral hiss-like structures, and thus an ambiguity in their origin exists. Swarm Alpha and Bravo observe auroral hiss with similar structure during the same time windows when simultaneously running the ASM burst-mode. These features are relatively intense in power with [A] in Figure 5 demonstrating a peak spectral density power of 11.08 pT/Hz^2 and [B] 9.27 pT/Hz^2. As expected, away from equatorial regions, no plasma bubbles are present in the IBI product during auroral hiss. Despite this, we cannot rule out the generation of signals due to rapid perturbations in the local plasma density.

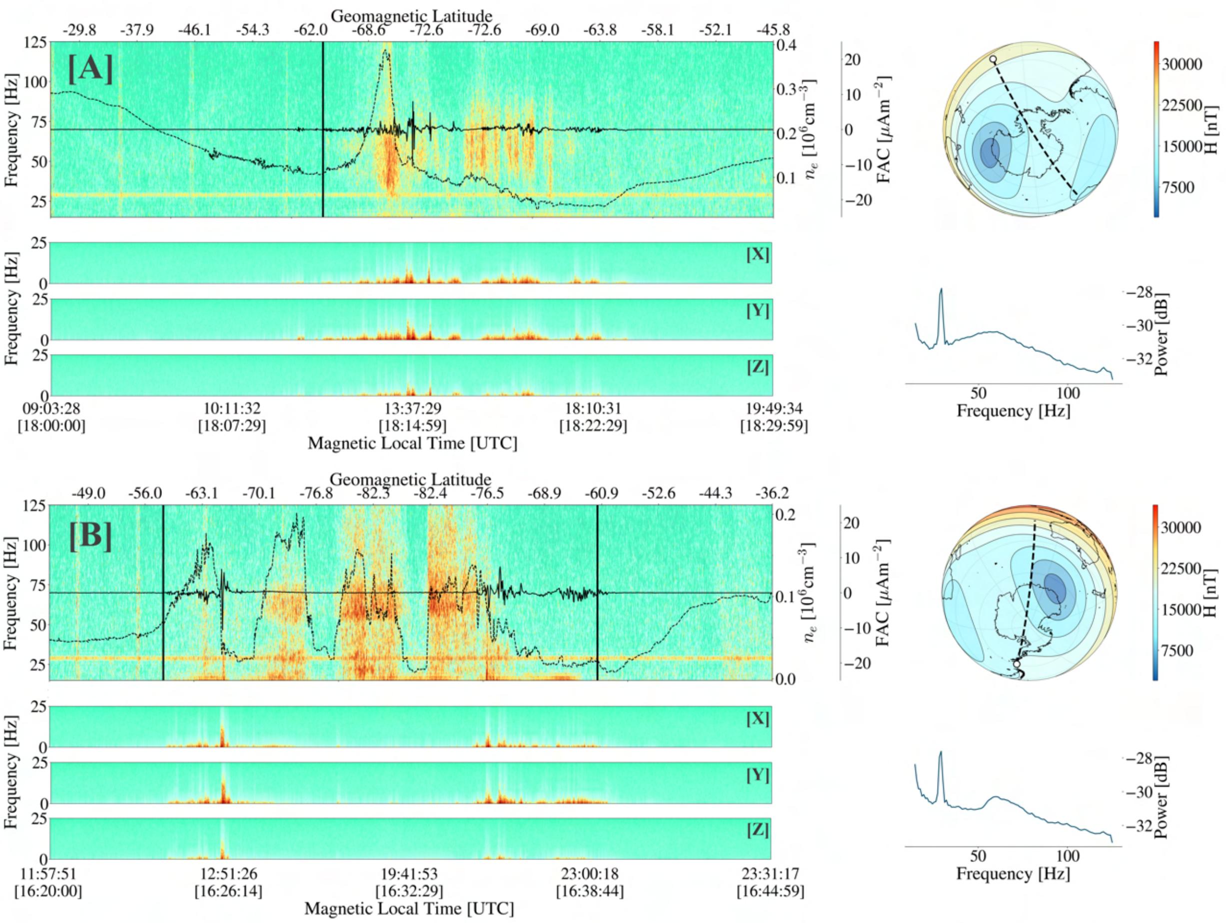

Fig. 5. Spectrogram of Swarm Alpha data showing examples of auroral hiss in Swarm Alpha associated with [A] field aligned currents (Kp=2-) and [B] during electron density irregularities (Kp=4), observed to strongly modulate the signal. See Figure 3 for further details. Spectrograms of the 50Hz vector components from the VFM instrument are also shown, labelled [X], [Y] and [Z].

We also note enhancements of auroral power in combination with FACs at lower frequencies i.e. < 25 Hz. This is highlighted by the Swarm VFM sensor vector data, whose power spectra are also plotted, with the observation that the vertical component has lower power. In the ASM data there are occasional bursts of energy that also exclusively span ~75-125 Hz that form relatively discrete spectral signatures. In general, the power peaks between 60 Hz and 100 Hz. The examples of auroral hiss that we find appear irrespective of the K_p value and do not depend on the plasma density magnitude, although sudden dips in plasma density are observed sometimes to fully attenuate hiss.

Therefore, large FAC magnitudes are not a guarantee that auroral hiss will be observed and the plasma density sometimes has an important role too. Diamagnetic plasma-density-driven spectral signatures are found in the Swarm 50 Hz vector data (Kim et al., 2020) but we do not always observe coeval rapid density variations.

Auroral chorus is another separate phenomenon and may be loosely discriminated from hiss via finer scale spectral structures (Golden et al., 2009), which we do not find in the Swarm observations over polar regions discussed here. However we do find the higher frequency signals between ~75 and 125 Hz sometimes show chorus-like small-scale structures, possibly suggesting two separate phenomena. Thus, there may be multiple different mechanisms acting to produce both the lower and higher frequency signals we observe, linked to one, or a coupling of, the contemporaneous FACs and density irregularities.

Equatorial plasma bubbles are a nightside phenomenon caused by a Rayleigh–Taylor instability when the ionospheric E-region exhibits ion recombination at a rate greater than the above F-region (e.g. Spogli et al., 2023). Small-scale depletions in the plasma density then arise due to a combination of the interacting electromagnetic and gravity fields. This phenomenon is often called equatorial spread-F. This results in the manifestation of high-power, broadband incoherent electromagnetic signals in spectrograms, as in Figure 6. These signals should not be misinterpreted as waves, but instead result from a diamagnetic effect. The ionospheric bubble index is generally, though not always, found to correlate well to these signals. The IBI relies on the vector magnetometer (VFM) 50 Hz mode which has a higher noise floor than the ASM.

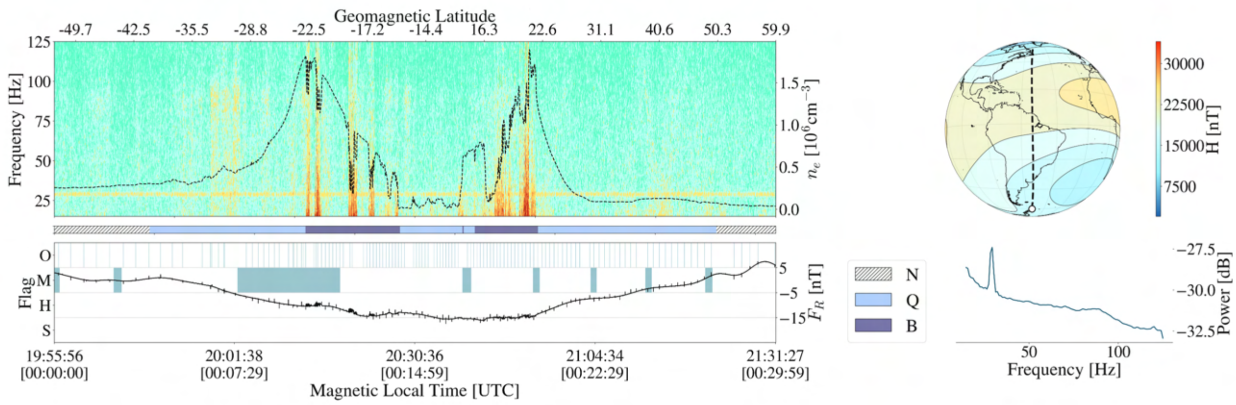

Fig. 6. Spectrogram showing an example of equatorial plasma bubbles in Swarm Bravo burst-mode data on 12-Dec-2023, seen as broadband high-power (orange/red) features coeval with rapid plasma density (dashed line) variations. Refer to Figure 3 for details of all additional datasets shown.

Correlation to IBI provides further evidence of a diamagnetic origin, as this product explicitly uses the presence of diamagnetic effects in its calculation (Park et al., 2013; Rodríguez-Zuluaga et al., 2017). That is, bubbles are only identified when coeval plasma and magnetic field irregularities persist.

3.3. Long lasting signals: Sweeps, Arches and Bowls

Whilst the utmost care is taken to limit unwanted noise from the functional electronics during design and build of the satellite, it appears likely that onboard interference produces artificial signals in the burst-mode data. Data flags associated with the onboard heater activity, when the magnetic conditions of resonance with the ASM are reached, correlate with short period (1-5 seconds) linear chirps (intense V-shaped signals), which have been documented by Léger et al. (2015). There are, however, further artefacts within the dataset which are yet to be attributed to a specific or known mechanism.

We find longer lasting linear and quadratic chirps extremely commonly within the spectrograms of the dataset (Fig. 7). Analysis of the flagged heater-driven linear chirps in data show that these signals are distinct from the longer-lasting sweeps we show. Heater related sweeps are much shorter in duration, higher in power and usually show a symmetric pattern about the flagged interval mid-point. The long period chirps we describe do not have a known origin. Based on their appearance, we name them 'sweeps' (V-shaped) and 'arches' (Λ-shaped), respectively. The labelled arch (A) and sweep (S) in Figure 7 have peak spectral density powers of 2.77 pT/Hz^2 and 3.91 pT/Hz^2, respectively. Quadratic arches are far less common than linear sweeps and on a typical day only 1-4 arches are recorded compared to sometimes 100+ sweeps. These spectral signatures usually have weak intensity but are long-lived signals visible above the background noise level of the ASM. The sweeps start at frequencies above the Nyquist frequency (125 Hz) and linearly decrease in frequency over a period of a few to tens of minutes, before reaching below 15 Hz and rising again to the Nyquist frequency, often taking the same time to rise as they took to decline. Occasionally, the sweeps do not extend below 15 Hz but plateau at a higher frequency (50 Hz, say) and then rise back to the Nyquist frequency. These are termed 'bowls'. Arches rise from below 15 Hz and increase in frequency to some high value (e.g. 100 Hz) before decreasing again i.e. these are essentially 'upside-down' bowls. Arches are often, but not always, bounded by sweeps. Examples of sweeps, arches and the ~29 Hz aliasing are shown in Figure 7, which also shows 60 Hz PLHR over North America.

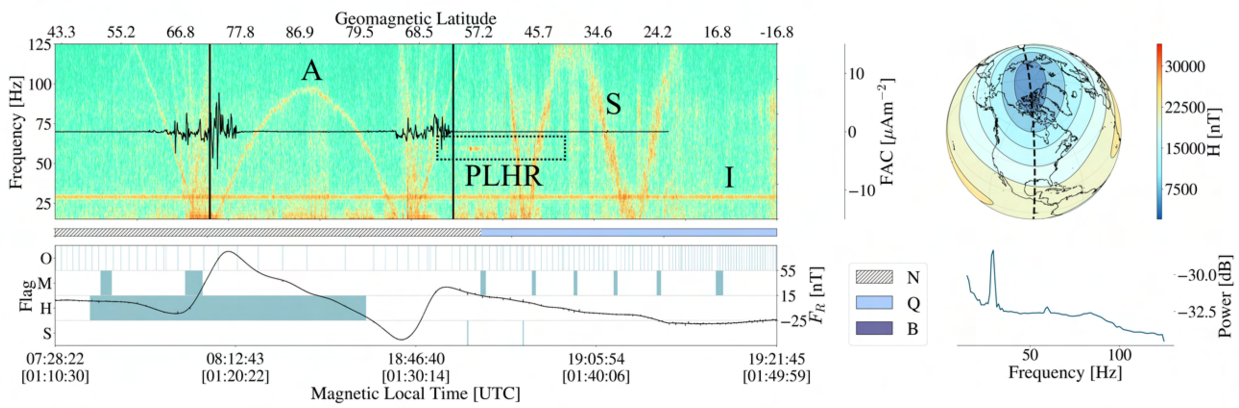

Fig. 7. As for Figure 3, a spectrogram showing an example of sweeps (S), an arch (A) and the onboard ~29 Hz instrumental aliasing (I) for Swarm Bravo on 09-Feb-2014. Powerline harmonic radiation (PLHR) is also highlighted.

Despite extensive investigation, there is little obvious temporal or spatial trend or correlation in these signals with location, time or other datasets nor between the Swarm satellites themselves even when in close proximity. Sweeps/arches can last tens of seconds to tens of minutes and have been observed up to half an orbit in duration. In addition, signals may also have both linear and quadratic components in spectrograms and several signals can often occur simultaneously, overlapping in time and frequency. We have found a number of instances whereby a train - or sometimes a single identifiable instance - of sweep features with an identical spectral signature and similar temporal extent can be observed, separated by some varying time interval. However, these repeated patterns are relatively uncommon across the dataset. The unique repetitions found thus far are on both the dayside and nightside of the planet, can occur over an entire day and span multiple burst sessions over different years. Some of these sweep trains are found to be mirror-images on successive occurrences, but their centre points show no obvious geophysical or geographical significance. Additional patterns also persist, and for example pairs of sweeps seen on successive orbits have been observed to merge into an arch, and bowls have been seen in at least two examples to appear to sink to 0 Hz and fold back into the spectrogram as arches. Longer lasting continuous signals (≥15 minutes) with both linear and quadratic components are rare, but when they occur, are found to be repeated across most or the entirety of a day with modulated structure orbit-on-orbit. Examples of these phenomena are provided in the supplementary material.

We speculate that these signals could be due to an unrelated on-board satellite system. One possible explanation could be related to an electronic component sensitivity to small temperature fluctuations somewhere in the craft; but no robust indication as to their origin has been identified. Across dozens of burst sessions, the occurrence, abundance, power, and duration of sweeps differ, so no clear trend has been identified. No relationship or correlation to the ASM Flags has been discerned either. We have also cross-checked the signals during conjunctions when Swarm satellites have been in close proximity (as at mission start or during later counter-rotation passes) without finding common occurrences at the same locations.

3.4. Equatorial Dispersive Waves

Dispersive wave-like signals over the geomagnetic equator lasting 10-30 seconds that are similar to whistlers, in regards to their descending-tone nature, are also observed; we have documented 20 clear examples thus far. Observations have been made during both day and nightside orbits. These signals appear to be related to the equatorial ionisation anomaly (EIA), illustrated in Figure 8 by the characteristic peaks in the plasma density that straddle the magnetic dip equator. The two signals shown in Figure 8, labelled D_1 and D_2, have peak spectral density powers of 4.31 pT/Hz^2 and 6.81 pT/Hz^2, respectively. They are possibly whistler-mode waves/chorus modulated or trapped by the local plasma environment. Both Swarm Alpha and Bravo have detected these signals. Figure 8 shows an unusual case of near-symmetric examples occurring over the EIA crests corresponding to each magnetic hemisphere, at approximately the same magnetic latitude. In this example, we also find that the signal labelled D_2 appears to have a break in its structure. Generally, whistlers last just 1-2 seconds, making these signals unusual or entirely unrelated. The enhanced spectrograms (tuned to increase the temporal resolution) in Figure 8 possibly also demonstrate contemporaneous short-period whistlers, with the event labelled W marked as a whistler in the Level 2 Swarm ASM whistler detection product (Hulot et al., 2022). More complex signals over the dip equator while the EIA is present are also observed in the data but with more diffuse spectral signatures and less obvious structures. Their origins are also unknown.

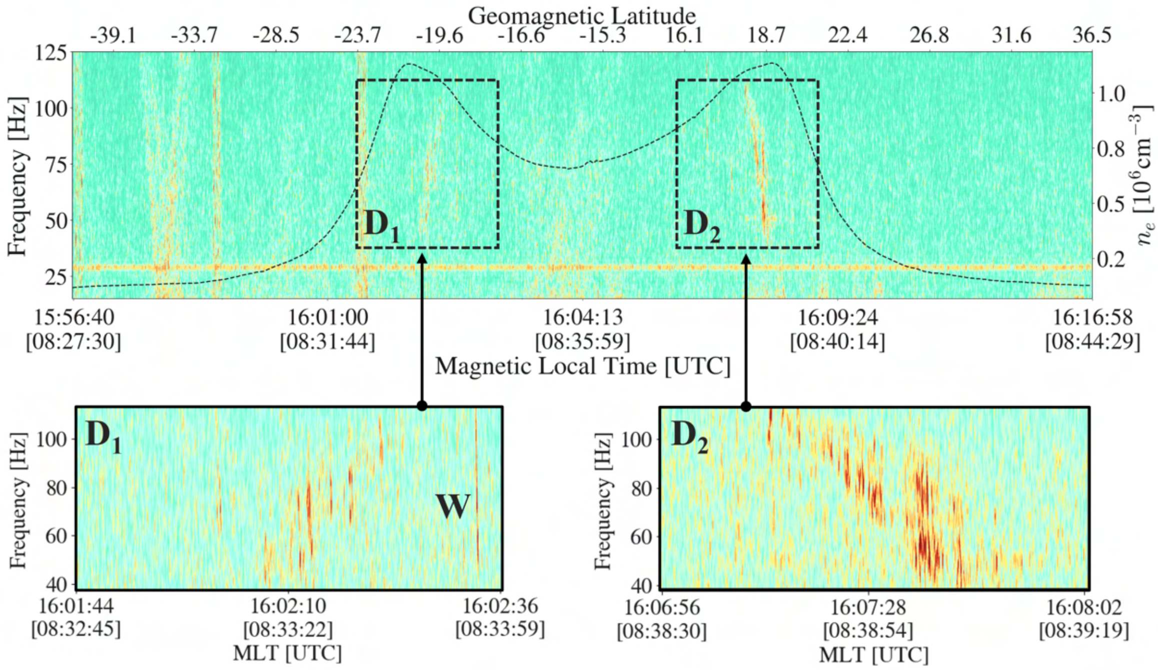

Fig. 8. Spectrogram showing an example of semi-symmetric dispersive signals over the South China Sea (D_1 and D_2) bordering the magnetic dip equator observed in Swarm A burst-mode data on 12-Aug-2022. The in-situ plasma density (dashed line), shows the equatorial ionisation anomaly as two distinct crests. Each signal is enhanced in the bottom panel by adjusting spectrogram parameters to increase temporal resolution. A lightning-generated whistler (W) is also marked.

3.5. Antarctic Hiss

Across 72 days from 2014 to 2023, magnetic wave-like features are observed at geomagnetic latitudes -40° to -75° over the South America/South African edge of Antarctica. We document a total of 94 examples from an analysis of all burst sessions in this period. They have a characteristic signature, rising in tone towards the auroral oval boundary. The signals last 1-5 minutes, starting at frequencies around 60-80 Hz before rising to 100-125 Hz, approximately linearly over time. Signals last 170 seconds on average, rising at a rate of 0.13 Hz/s. In almost every case, the ascending tone cuts off before reaching the auroral oval boundary. The signals are observed by all three craft. A single simultaneous observation is fortuitously found in both Swarm Bravo and Charlie on 02-Feb-2014, when both satellites were still in an orbital configuration where they were following each other, before the manoeuvres to separate them to different altitudes. This provides evidence of an unknown, but geophysical, origin.

Figure 9 shows two examples of the signal (labelled R) in spectrograms from Swarm Alpha [A] and Bravo [B] in the panels; their peak spectral power density is 3 pT^2/Hz and 6 pT^2/Hz, respectively. Figure 10[A] plots the location of the most poleward location of each example and indicates interpreted signal aliasing by those coloured black. We find that where signals alias/fold back into spectrograms, they follow the local cyclotron frequency if it were to also alias upon reaching the Nyquist (see supplementary material). Also shown as shading is the median absolute value of the Swarm-derived FACs using data during only days where signals are observed; here we calculate the FAC absolute values over the 24 hours of each date where signals are found and plot their median values in 5°×1.5° longitude/latitude spatial bins. Most signals occur outside or on the edge of FAC activity. Field magnitude (F) contours are also shown, calculated from the CHAOS-7.17 model on 01-Jan-2022, demonstrating the offset of the magnetic pole. Panel [B] shows the event MLT/magnetic latitude distribution in 1 hour by 7.5° degree bins. A post-noon, pre-dawn bias is observed.

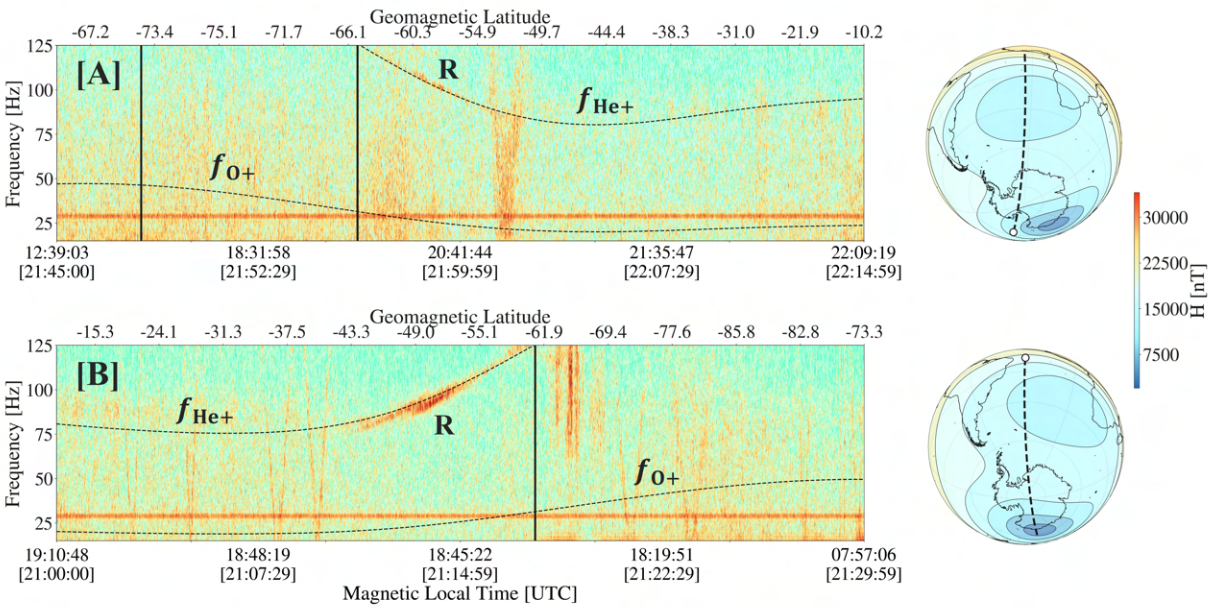

Fig. 9. As for Figure 3, showing examples of rising tone signals (R) observed by Swarm Alpha and Bravo on 21-Sep-2021 [A] and 23-May-2023 [B], respectively. The local ion cyclotron frequencies of He^+ (f_{He+}) and O^+ (f_{O+}) also plotted as dashed lines.

There is no clear correlation to K_p values prior to, during or after events, suggesting elevated geomagnetic activity is not a prerequisite to observations. Our sample size is however limited. Data from burst sessions in 2023 show the clearest examples with strong power. A spatial bias is observed, whereby events are clustered between longitudes -70° to 60°, poleward of the South Atlantic Anomaly (SAA) region. Preliminary investigations suggest He^+ band electromagnetic ion cyclotron (EMIC) waves may be a potential source. However the observation of waves at the local ionospheric gyrofrequency, rather than that of compressional waves from a magnetospheric source (~0.1-5 Hz) suggests ionospheric hiss rather than EMIC waves originating in the outer radiation belt. Signals are found to sit predominantly between L-shells 1-8, with a mean value of ~6. This is similar to the observations of EMIC waves seen by the Van Allen Probes (Sigsbee et al., 2023).

Ross et al. (2021) demonstrate that He^+ band EMIC waves measured by the Van Allen Probes in particular have a strong post-noon and pre-dawn MLT bias, which we also observe in Swarm data. Their study also shows a correlation between event rate and solar wind dynamic pressure

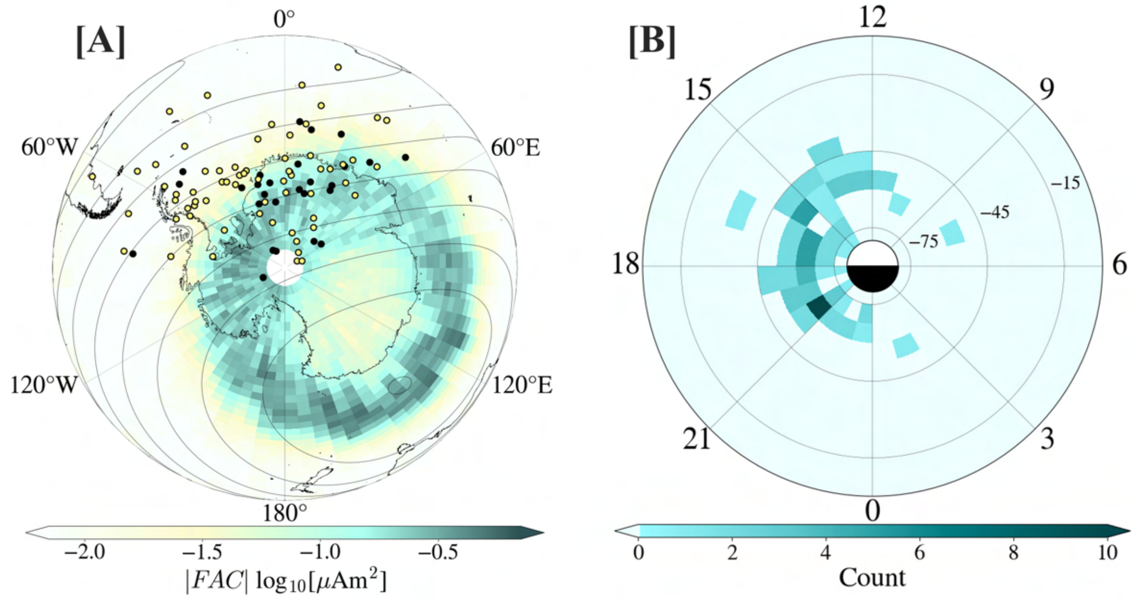

Fig. 10. [A] Spatial distribution of all Antarctic wave events documented, with those showing interpreted aliasing at the Nyquist ceiling in black and yellow otherwise. Also shown as shaded spatial bins are the median absolute values of the Swarm-derived FACs using data only from days where signals are observed. [B] Magnetic local time (MLT) vs quasi-dipole latitude distribution of events in 1 hour by 7.5° degree bins.

(P_{dyn}). Using the 1-minute cadence OMNI solar pressure data derived at the magnetospause, we find events occur while the contemporaneous 24-hour solar pressure has a median of 2.6 nPa. Quiet time conditions are in the range 0-3 nPa and thus we only consider pressures exceeding 4-5 nPa to be unsettled. The median peak pressure in general is usually higher at ~3.6 nPa. We find 79 signals occur where the peak P_{dyn} is greater than 2 nPa, 26 of which occur for peak $P_{dyn} > 5$ nPa. Though we find no evidence of a correlation to dynamic pressure so far, the sample size is small. The observed geographic clustering is intriguing and the location of the south magnetic pole and its distance from the SAA may play a role. The SAA is the only region where the field strength is low enough for $f_{\mathrm{He+}}$ to occur below 125 Hz. As a result, the longitude and hemisphere bias are probably a result of the instrument bandwidth.

EMIC waves observed in Swarm 50 Hz data show a similar geographic bias in the southern hemisphere (Wang et al., 2022). However, the MLT distribution is not similar and the frequencies are lower, matching magnetospheric cyclotron frequencies. The poleward bias of events could suggest FACs or phenomena associated with the local L-shell values are important, as we do not see events at lower latitudes. Oscillations at ionospheric gyrofrequencies also suggest a non-magnetospheric wave source and instead local ionospheric generation. A study by Xia et al. (2019) using DEMETER satellite data demonstrates that ionospheric hiss wave power at frequencies close to the local proton gyrofrequency is strongest in the region poleward of the SAA. This is also what we observe, although in the He^+ band. Hu et al. (2024) discuss ionospheric hiss at the local proton gyrofrequency in CSES satellite data, and show spectrogram features that are similar in characteristic to those which we find for Swarm. Zhima et al. (2017) suggest that high-altitude plasmaspheric hiss is a viable generation mechanism for lower-altitude ionospheric hiss; ray-tracing investigations may better indicate whether the EMIC source region could also be responsible for hiss events. New measurements with a sensor of greater bandwidth than 250 Hz would help resolve the source of this signal.

3.6. Quasi-periodic Diffuse Interference

A quasi-periodic (QP) diffuse interference centred around 89 Hz is observed in the data. An automated detection was used to investigate its occurrence. The signal exhibits a beating pattern in many examples, with regular enhancements and depletions of energy, as shown in Figure 11. Peak spectral density power in this example is 2.77 $\mathrm{pT/Hz^2}$. The beat period is not consistent, varying from 20 to 90 seconds, sometimes showing a pattern in which it decreases, and then terminates entirely. Not all days exhibit any visible 89 Hz interference, but on those that do we find it occurs primarily over the South Atlantic Anomaly.

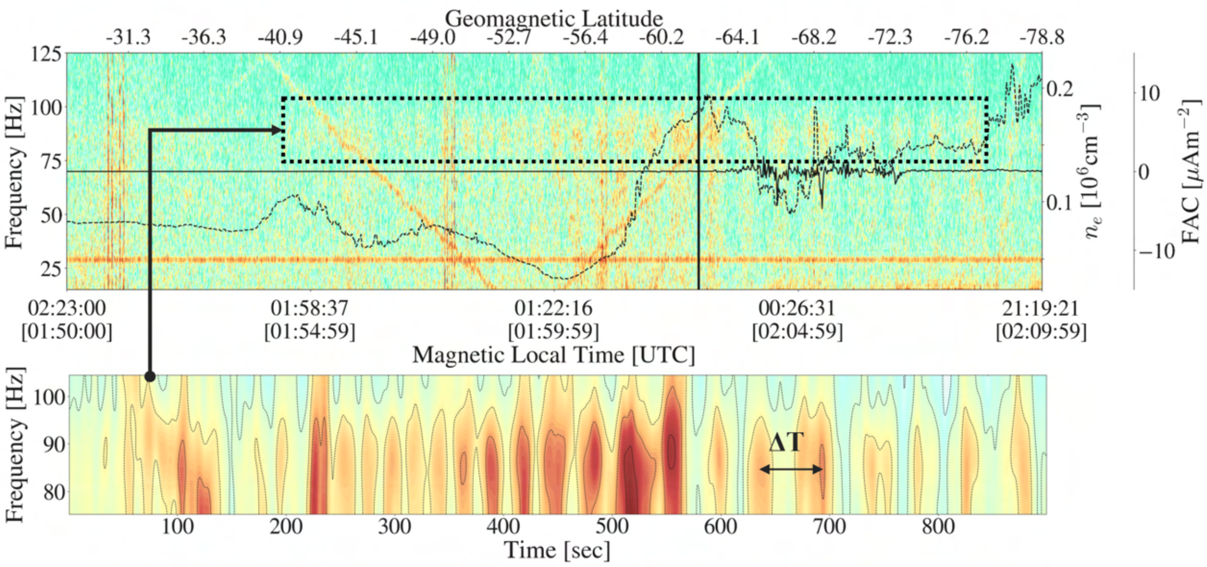

Fig. 11. Top: As for Figure 3, an example of quasi-periodic diffuse interference centered around ~89 Hz. Bottom: Visually enhanced plot of the quasi-periodic structure of the interference created by tuning spectrogram parameters and applying smoothing to the dashed region in the top panel spectrogram. The period of interference beating, ΔT, is seen to vary.

To map the occurrence of the QP diffuse signal within the 78 to 100 Hz band, we subtract the deviation of power spectra intensity from the local linear trend in Figure 12 over 30 second windows, using all burst-mode data available from 2020 to 2021 for Swarm Alpha and Bravo, thus using data spanning 290 days and all local times. This is done by [1] binning the data into 30 second (~235 km) time-windows on a given day; [2] computing the median spectrogram power for each frequency bin; [3] truncating the result to the band 70-110 Hz and locally detrending using a linear fit to find the deviation from the background power; [4] summing the resulting power deviation as fitted by a quadratic curve to the band 78-100 Hz; and then [5] taking the percentage of values whereby this sum exceeds 0.75 $\log_{10}(\mathrm{nT}^2/\,\mathrm{Hz})$ in spatial latitude/longitude bins. The value of 0.75 was manually chosen based on when interference is visible in spectrograms above background noise. Windows in which the fitted curve had a non-negative quadratic coefficient were assigned a power of zero to better remove background noise.

From Figure 12, the quadratics fitted to each window reveal a central frequency of 88.85 Hz, although the method is sensitive to the exact choice of frequency band over which detrending and curve fitting are done. We observe a clear correlation between the event occurrence and the total magnetic field strength, with the interference centered on the South Atlantic Anomaly, even when the frequency bands in our method are varied. The signal appears to be confined to regions where magnetic field strength is below 30,000 nT. Finally, no magnetic local time or seasonal trends were found to be associated with the interference.

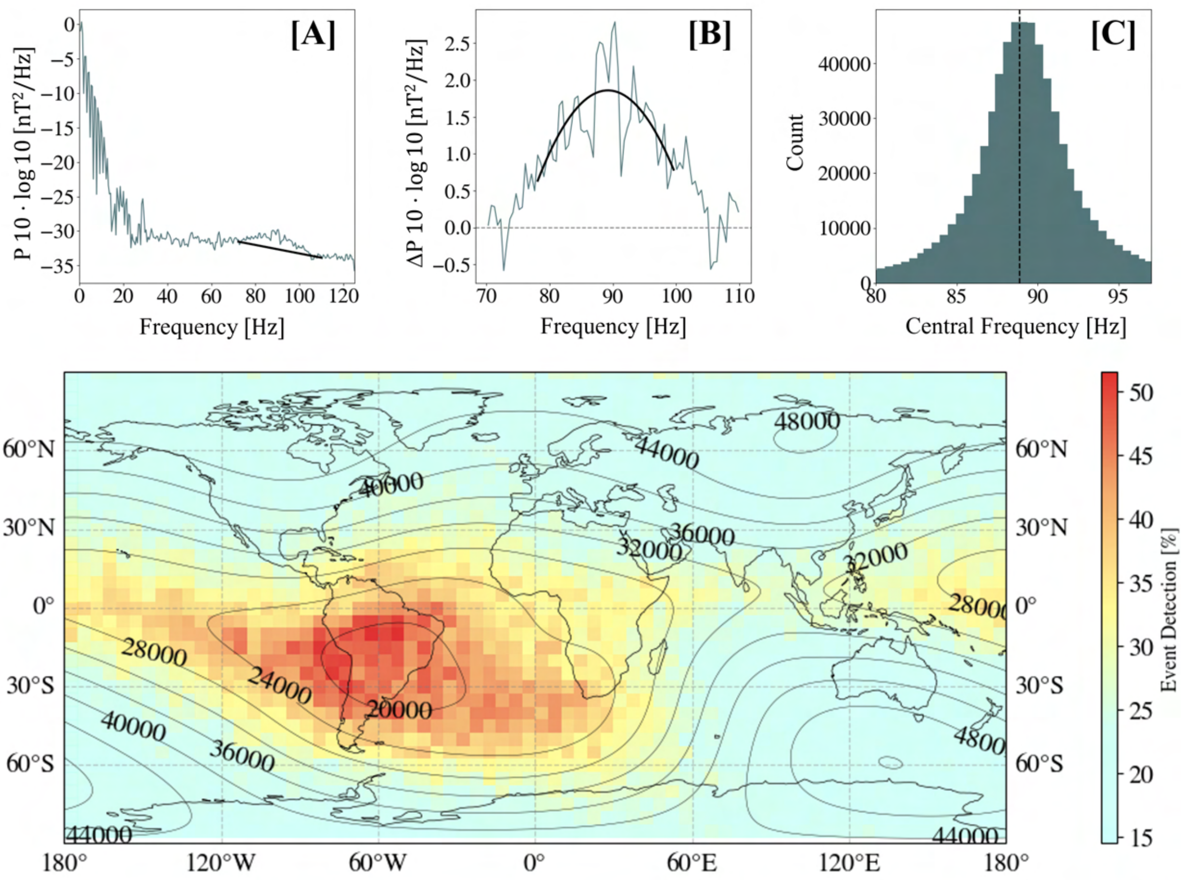

Fig. 12. Spectral interference events binned in 5°×5° spatial windows. All burst-mode data from 2020 and 2021 are used for both Swarm Alpha and Bravo (spanning 290 days). 30 second time-windows for each day were used to compute power spectra, detrended over the band 70-110 Hz [A], and then in each detrended window we fit a quadratic to the 78-100 Hz range [B], from which we can also find the central frequency over all peaks [C]. The labelled (in nT) contours are total field intensity on 01-Jan-2021 at 500 km altitude.

3.7. Hooks

Hook-like signals (Fig. 13) are seen consistently in the data in 2014 and 2019-2023 during magnetic local times (MLTs) around 0900 and 1500, mostly confined to low-latitudes. We document a total of 385 signals across 16 burst-sessions, 287 of which occur around MLT 1500 and 98 during MLT 0900. Only 5 are observed in 2014 and 2 in 2019, although burst-sessions are extremely limited in these years. In a burst campaign on Swarm Alpha during October 2023, 81 signals are found across just 7 days. In total, 236 observations are made by Swarm Alpha and 147 by Bravo. Their origin is assumed to be geophysical though a mechanism is yet to be identified. Hooks appear around 80-110 Hz as narrowband intense signals, starting at a lower frequency, rising slowly by around 10-20 Hz before falling back to close to their original frequency. Two examples are shown in Figure 13 with peak spectral density power 2.63 pT/Hz^2 [A] and 2.97 pT/Hz^2 [B]. Sometimes hooks also show the inverse behaviour. They usually last 2-5 minutes, but can extend for up to 20 minutes.

In the numerous examples observed in 2022, hooks nearly always terminate at the magnetic dip equator. During 2023, hooks are seen to extend across the dip equator and also persist at mid-latitudes. The length and power of these signals is possibly increasing in correlation with the solar cycle with the hooks found in 2019-2021 often less than 1 minute in duration. We cannot however rule out their termination instead relating to the satellites leaving the strict local time windows in which hooks are preferentially observed, with short-lasting events also observed in 2023. Remarkably similar-looking signals have been detected at ground observatories in California (Sentman and Ehring, 1994), Taiwan (Wang et al., 2005), Alaska (Heacock, 1974) and the South Pole (Kim et al., 2006). The temporal sampling bias of burst-mode data limits solar cycle analyses. To our knowledge, it is the first time satellites have observed these narrow-band signals.

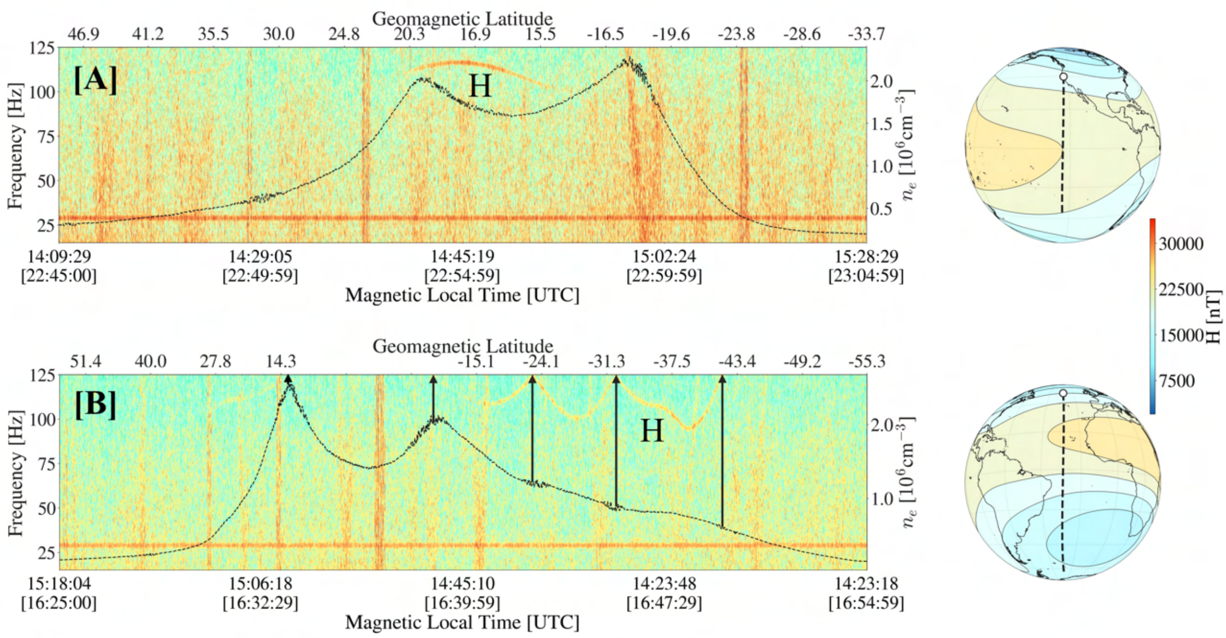

Fig. 13. As for Figure 3, an example of [A] a typical hook-like signal (H) observed in Swarm burst-mode data and [B] demonstration of contemporaneous plasma density (dashed line) irregularities and modulation of a long-lasting hook. Both examples are from burst-mode data on 05-Oct-2023.

Serendipitously, a simultaneous event was found in 2014 (Fig. 14), after the launch phase when each satellite was in a similar orbit and the ASM on Swarm Charlie was still operational. In each dataset, the hooks are seen to reach the 125 Hz ceiling and alias or fold back in frequency. The MLT for each craft at this point is around 09:38. There is a time lag of several minutes between the event being observed by Alpha/Bravo and Charlie, which is to be expected since Charlie trails behind Alpha/Bravo. In the MLT frame, this lag is only around 20-30 seconds. Each craft travels at approximately 7.8 km/s, and so the distance over which hooks are recorded spans around 1350 km. These signals thus persist over extremely large distances. Spectral density power for each hook peaks at 2.22 pT/Hz^2, 2.34 pT/Hz^2 and 2.01 pT/Hz^2 in Swarm Alpha, Bravo and Charlie, respectively.

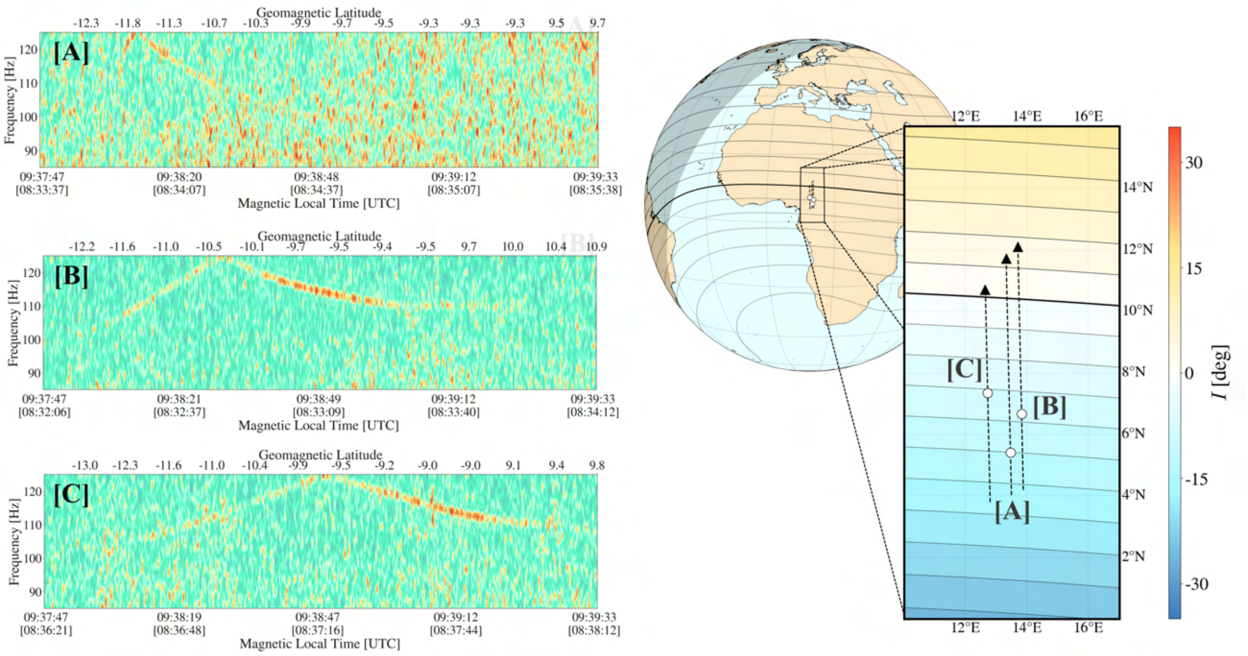

Fig. 14. Left: Detection of the same hook-like signal observed on 19-Jan-2014 at the same altitude, for Swarm Alpha [A], Bravo [B] and Charlie [C]. Spectrogram panels are aligned by magnetic local time and the power scale fixed to allow comparison of each event. Right: Inclination (I) calculated at 500 km altitude, with the zero contour shown as a thick black line. White points indicate the location corresponding to where each hook is seen to alias upon hitting the 125 Hz Nyquist frequency. Satellite tracks are shown by dashed arrows.

In the burst-mode data from 2023, there are multiple examples where irregularities in the in-situ plasma density data coincide with modulation of hooks. This is shown for a particularly long-lasting event that extends into mid-latitudes in Figure 13. The absence of broadband signals associated with density irregularities described previously is not of concern, as there are many examples of plasma irregularities without coexisting spectral features. If these density perturbations are artificial, this suggests hooks also may be, but the overall evidence found thus far suggests a geophysical origin is more likely.

4. Discussion

4.1. Signals of Known Origin

Onboard interference produces known artefacts in the burst-mode data including a stable ~29 Hz band which is always present, and short duration (1-5 second) linear sweeps which result from cross-talk when the ASM heater is active at specific values of the ambient magnetic field. These signals are understood and are not the focus of this study of the burst-mode data.

4.1.1. Powerline harmonics

Powerline harmonic radiation (PLHR) from high voltage power networks is seen as stable 50/60 Hz lines in spectrograms and is thus far only observed in spectrograms during nightside orbits while quieter ionospheric conditions persist. Preliminary statistical analysis using 2020-2021 data suggests PLHR events are observed on almost all days, and that dayside detections do occur but are too weak to be visible in spectrograms. Corresponding 100/120 Hz harmonics are not observed. Wave-plasma theory suggests that PLHR should reflect off the lower ionosphere, owing to emissions occurring below the local plasma frequency; however, leakage into the ionosphere contradicts this expectation. The stronger presence of PLHR during nightside conditions can be attributed to reduced wave attenuation under decreased plasma density. PLHR has been observed, though relatively infrequently, in satellite missions such as DEMETER (e.g. Parrot et al., 2014), C/NOFS (e.g. Pfaff et al., 2014), Chibis-M (e.g. Dudkin et al., 2015) and CSES (Zhao et al., 2022).

The spatial distribution of events closely aligns with CSES findings (Liao et al., 2024) and we also find Northern Europe shows elevated PLHR intensities, consistent with the findings of Zhao et al. (2022). Our temporal results support Němec et al. (2008), which observed stronger PLHR on the nightside. However, Liao et al. (2024) report a dayside bias based on third harmonic analysis, indicating some inconsistency across studies. While PLHR detection criteria were not fully explored here, the Swarm mission could improve modelling of PLHR leakage. ELF transmitters, including Russia's 82 Hz ZEVS, are also present, and are observed by DEMETER (Pilipenko et al., 2019).

4.1.2. Auroral Hiss and Equatorial Plasma Bubbles

Auroral hiss, associated with strong field aligned currents and plasma density irregularities within the auroral oval, as well as equatorial plasma bubbles (EPBs), associated with small-scale depletions in the equatorial nightside plasma, are known geophysical effects. They are clearly observed in the burst-mode data. Their peak spectral density power is far greater than other signals we observe, at around 10 pT/Hz^2; other signals range from 1-6 pT/Hz^2. EPBs have previously been demonstrated in Swarm burst-mode data by Coïsson et al. (2015). The Swarm ionospheric bubble index product correlates well with the EPB signatures seen in spectrograms, supporting a diamagnetic spectral origin over a wave source (e.g. Alfvén waves). Broadband emissions detected over EPBs are also found in CSES measurements, including within the same frequency range as Swarm, from electric field data (Gou et al., 2023). Auroral hiss (AH) is largely incoherent and lacks finer-scale structures which would imply chorus waves as an origin.

Our results find AH is often banded between ~60 and 100 Hz and is observed around twice as often in the southern hemisphere. There does not appear to be an obvious dependence on the K_p

index. Most studies focus on higher frequency examples in the kHz-MHz range, however Lühr and Zhou (2023) note the presence of low frequency FAC-driven signals in Swarm 50 Hz data, which we also find. Bands of power also persist locally outside auroral zones and are often coeval with plasma density irregularities. Our limited sample size restricts robust temporal analyses. Investigations into the spatial extent and fine-scale structures of plasma bubbles are however suggested to be made possible by the burst-mode data and simultaneous burst campaigns on different craft could improve current knowledge.

4.2. The Unknown

We find multiple examples of signals in Swarm ASM burst-mode data whose sources remain unknown. From our analysis we suggest that sweeps and arches are non-geophysical, probably being related in some manner to instrumental, electronic or spacecraft interference. We focus on three longer-lasting signals believed to be geophysical in origin: (1) hooks, which are observed consistently at MLTs 0900/1500 during 2014 and 2019-2023; (2) equatorial dispersive waves and (3) rising tone signals over the Antarctic.

4.2.1. Hook-like signals

Hooks are mostly confined to low-latitudes, occur during MLTs 0900/1500 ±30 minutes, and last 2-5 minutes. We find most examples (287 of 385 documented) occur at MLT 1500. Numerous examples in 2023 also last up to 20 minutes and extend into higher (±50/60° magnetic) latitudes. A simultaneous detection across all three craft in 2014 (Fig. 14) provides evidence that hooks are geophysical in origin. Further evidence of their geophysical origin comes from ground-based measurements in Alaska (Heacock, 1974) and the Antarctic (Kim et al., 2006), mid-latitude measurements (California, USA) (Sentman and Ehring, 1994) and low-latitude measurements in Taiwan (Wang et al., 2005) which show similar signals with the same temporal structure as hooks and in the same frequency band as that seen in Swarm data. Fritz et al. (2018) noted the dependence on the relative solar angle for Antarctic hook-like signals. If we assume a shared source for Swarm and ground observations, we could expect hooks outside the relatively strict MLT windows (0900/1500 MLT) in which they are observed by Swarm. Wang et al. (2005) demonstrate a local time bias closely matching hooks observed by Swarm satellites in the low-latitude (23.47°N) measurements recorded at the Lulin Observatory in Taiwan; hooks are detected at low-latitudes in all but rare cases in Swarm data. The results shown at Lulin suggest we should also observe hooks at 2000 MLT, which we do not.

Hooks in Swarm data are detected over 1000+ km distances, possibly suggesting a large-scale phenomenon rather than lightning-generated whistlers as proposed by Kim et al. (2006). There is however ambiguity caused by the unknown temporal/spatial scale of wave measurements. In the example where simultaneous detection across all craft is seen, the observation time-lag in UTC between each craft suggests a westward propagation of the signal, implying a travelling wave of some description rather than a standing wave. Alternatively this could be a standing wave event drifting with time. Mid-high latitude examples are rare in Swarm data despite the Antarctic station detecting a large number of such signals. Further investigations are required to identify the origin/mechanism of hooks and targeted burst campaigns, with the aim of conjugate event detections by making use of the observed local time and spatial biases, may provide better statistics.

4.2.2. Equatorial Dispersive Waves

Dispersive features over the geomagnetic equator are seen across numerous burst-sessions in both Swarm Alpha and Bravo data, with ~20 clear examples documented thus far. A possible relation to the equatorial ionisation anomaly is suggested, given it is persistent in all examples. In exceptional cases, symmetric signals are found at each plasma density crest, whereas in most examples features are seen on only one side of the dip equator. Such signals last up to 30 seconds, far longer than most lightning-generated whistlers, but not unprecedented. Despite being longer-lasting, these spectral signatures may still originate from or be related to lightning/chorus emissions and sometimes precede or follow low-latitude whistler events. We also note that hooks sometimes demonstrate dispersive tails, dipping down to ~60 Hz, further suggesting that they might be related to whistlers. It is possible both signals have a shared origin, or their dispersive characteristics result from the same local geophysical environment. However, this seems unlikely, given that occurrences of dispersive waves fall outside the local time window during which hooks are observed.

4.2.3. Antarctic Hiss

Rising tone signals observed over high-latitudes in the southern hemisphere across 2014 to 2023 are found to show no clear correlation to geomagnetic activity. Examples are found during both northward and southward orbits. There is an absence of any similar features in the northern hemisphere. The rising tones are found to occur equatorward of, rather than within, the auroral oval boundaries in the majority of the 94 documented cases. A spatial-bias is also shown to exist, whereby signals are clustered from -70° to 60° in longitude. This appears to relate to the SAA which spans the same sectoral region. Their rising tone structures correlate to the local ionospheric gyrofrequency band of He^+ ions, suggesting the detection of ionospheric hiss.

A mean L-shell value of 6 could suggest the outer radiation belts as the source region. This would imply an EMIC-driven wave mechanism. However, we would then expect frequencies in the range 0.1-5 Hz, reflecting a magnetospheric source origin. Instead, local ionospheric generation by an unknown mechanism could be more likely. Zhima et al. (2017) suggest a mechanism whereby high-altitude EMIC activity can trigger ionospheric hiss events at lower altitudes. In this case, plasmaspheric hiss may act as the trigger. Ray tracing simulations could better help understand these signals, as well as running more simultaneous burst-campaigns in order to find more contemporaneous observations between craft. A similar spatial bias towards the SAA region is found in DEMETER data for the local proton cyclotron frequency (Xia et al., 2019). The relatively low sample size of Swarm data limits more detailed statistical analyses.

4.2.4. Quasi-periodic Diffuse Interference

A band of diffuse power centered at ~89 Hz is observed in the burst-mode data, showing a strong bias towards the South Atlantic field low and often exhibiting a beating pattern. The period of beating is not consistent, and varies from 20 to 90 seconds, but is generally ~30-40 seconds. This quasi-periodic signal is absent on many days. Spectral analysis does not reveal the discrete sub-harmonics required to produce beating. This fact, in combination with the centre frequency not being an exact multiple of the known on-board aliasing, casts doubt on a harmonic origin. The spatial/temporal biases and beating pattern are not understood and further investigations are required. Quasi-periodic signals are demonstrated in CSES data by Zhima et al. (2020) and Hu et al. (2024), but at frequencies above the Nyquist in Swarm data, so it is unclear if they are of shared origin. Zhima et al. (2020) suggest whistler-mode wave-packets as an origin. Harmonics could be enhanced/modulated under conditions relating to the field strength over the SAA - as shown in Figure 12 - possibly due to an instrumental effect. Further investigations using multi-satellite data may better reveal the source origin.

4.2.5. Sweeps and Arches

Sweeps and arches are present throughout all burst sessions, though with varying strength, spectral signature, duration and abundance. Signals with both linear and quadratic components exist, often lasting tens of minutes. Additionally, these signals are regularly seen to overlap. There is no obvious trend in their occurrence, with little temporal or spatial bias yet discovered, though we found some patterns repeat for a few orbits. The lack of any geophysical pattern, and an absence of simultaneous events during satellite conjunctions, leads us to conclude that they are probably caused by an unknown instrumental interference effect, possibly sensitivity of some electronics to small temperature fluctuations; however this is speculation at present.

Similar looking features were found in CHAMP data by Yin et al. (2015). However they showed the features correlated to passing through points of zero declination, leading to tiny random oscillations in the analog-to-digital converter in the Y-component. As the ASM is a scalar instrument, and does not operate under the same principals, it is not obvious that the CHAMP noise-features could result from a shared phenomenon. We found that the noise floor of the Swarm vector magnetometer is too high, around $15\text{pT}/\sqrt{\text{Hz}}$ as reported in Merayo et al. (2008), compared to the power of sweeps/arches, so unfortunately it not possible to compare the ASM and VFM data. However, similar artificial V-shaped signals are also found to occur in the Macau Science Satellite-1a (MSS-1) vector magnetic data in the band 1-25 Hz, with a nightside bias (Song et al., 2025). The VFM onboard MSS-1 operates under the same principle as that onboard the Swarm satellites and the signals are observed in all three vector channels. Their origin in MSS-1 data is also ultimately unknown.

5. Conclusion

The absolute scalar magnetometers on board the Swarm satellite trio have proved capable of detecting novel ELF signals of unknown origin, as well as a host of known geophysical and man-made signals, when operating in an experimental 250 Hz burst-mode. Powerline harmonic radiation, ELF transmitter emissions, auroral hiss and plasma bubbles are known effects, and can be observed regularly in the data. Auroral hiss and plasma bubbles are found to correlate to irregularities in Swarm-derived field-aligned currents and in-situ plasma density measurements, respectively. Powerline harmonic radiation detection is most abundant during nightside orbits, during which ionospheric conditions are quieter and thus wave attenuation lower. Despite being known effects, the high quality nature of these data and their relatively high sampling rate means that further research opportunities are opened up. In particular, more detailed investigations into the spatial extent of plasma bubbles and additional understanding of why and when PLHR leaks into the ionosphere may be possible.

Unknown features include ‘sweeps’ and ‘arches’ which are linear and quadratic chirps found at all latitudes and longitudes, and are probably an effect caused by instrumental interference or possibly data processing, though no obvious trend has been discovered yet. Further work should be done to better understand these signals, so as to prevent their possible occurrence in future missions. In particular, the use of machine learning is suggested for mapping all sweeps and arches in the data for a thorough quantitative analysis.

Hook-like signals are observed around magnetic local times 0900 and 1500 over low-mid latitudes, and are remarkably similar to ground-based observations, suggesting they are a geophysical phenomenon. Their source mechanism is yet to be resolved and may indicate a gap in knowledge. Further, multiple examples of an unusual rising tone signal are seen close to Antarctica confined to south of the South Atlantic Anomaly region. Their origin could be linked to EMIC wave activity; however, this study finds that they follow the local ionospheric gyrofrequency of helium ions, $f_{\mathrm{He+}}$, rather than that of the magnetospheric EMIC source region, which we thus interpret as ionospheric hiss. We also find hiss with periodic diffusion and enhancement centred around 80 Hz primarily around the South Atlantic Anomaly and long period whistler-like waves at equatorial latitudes. Understanding the signals identified in this study may have broader implications for our knowledge of ionosphere-magnetosphere coupling and wave-plasma modelling.

Additional efforts are needed to determine the origin of and fully characterise all the signals we observe. As burst-mode data continue to accumulate, more comprehensive investigations and statistical analyses may uncover previously unknown ionospheric mechanisms. Additionally, with the peak of solar cycle 25 now having passed, future studies will have the opportunity to assess longer-term solar cycle trends. This study proves the value of high-quality magnetic missions and it is evident that there is immense scientific value in the ASM burst-mode data for detecting new ionospheric phenomena.

Acknowledgements. This research was funded by the ESA DISC-5 project. All data are publicly available (© ESA 2025) from the ESA Swarm Dissemination Server (https://swarm-diss.eo.esa.int/). This publication was approved by the Executive Director of the British Geological Survey (UKRI).

References

Chauvet, L., and G. Hulot, 2023. ASM Burst Product Definition for Operational Release of Data. *Technical Report SW-ASMV-DD-IPGP-0008*, IPGP. URL https://swarm-diss.eo.esa.int/#swarm%2FAdvanced%2FMagnetic_Data%2FASM_Burst_Mode_Data%2FDocumentation. 2

Coïsson, P., G. Hulot, L. Chauvet, L. Brocco, R. Madelon, et al., 2021. Investigating Lightning Generated ELF Whistlers to improve ionospheric models (ILGEW). *Deliverable 08: Updated ILGEW Dataset User Manual*. 1

Coïsson, P., L. Brocco, G. Hulot, J. M. Leger, T. Jager, P. Vigneron, F. Bertrand, and A. Boness, 2015. Analysis of Plasma Irregularities and Electromagnetic Signals Based on Swarm Absolute Scalar Magnetometer Burst Mode Sessions. AGU Fall Meeting. Poster, URL https://u-paris.hal.science/hal-04059798. 4.1.2

Coïsson, P., P. Deram, G. Hulot, J. M. Leger, T. Jager, and L. Brocco, 2016. Whistler-like Signals Detected Simultaneously by Swarm Satellites. In AGU Fall Meeting Abstracts, vol. 2016, AE33B–0447. 1

Dudkin, F., V. Korepanov, D. Dudkin, V. Pilipenko, V. Pronenko, and S. Klimov, 2015. Electric field of the power terrestrial sources observed by microsatellite Chibis-M in the Earth's ionosphere in frequency range 1–60 Hz. *Geophysical Research Letters*, **42**(14), 5686–5693. 10.1002/2015GL064595, URL https://agupubs.onlinelibrary.wiley.com/doi/abs/10.1002/2015GL064595. 3.1, 4.1.1

Finlay, C. C., C. Kloss, N. Olsen, M. D. Hammer, L. Tøffner-Clausen, A. Grayver, and A. Kuvshinov, 2020. The CHAOS-7 geomagnetic field model and observed changes in the South Atlantic Anomaly. *Earth, Planets and Space*, **72**(1), 156. 10.1186/s40623-020-01252-9, URL 10.1186/s40623-020-01252-9. 2

Fratter, I., J.-M. Léger, F. Bertrand, T. Jager, G. Hulot, L. Brocco, and P. Vigneron, 2016. Swarm Absolute Scalar Magnetometers first in-orbit results. *Acta Astronautica*, **121**, 76–87. 10.1016/j.actaastro.2015.12.025, URL https://www.sciencedirect.com/science/article/pii/S0094576515004671. 1

Friis-Christensen, E., H. Lühr, and G. Hulot, 2006. Swarm: A constellation to study the Earth's magnetic field. *Earth, Planets and Space*, **58**, 351–358. 10.1186/BF03351933. 1

Fritz, B. A., J. Heavisides, M. A. Young, H. Kim, and M. R. Lessard, 2018. ELF Whistler Dependence on a Sunlit Ionosphere. *Journal of Geophysical Research: Space Physics*, **123**(5), 3955–3964. 10.1029/2017JA024912, URL https://agupubs.onlinelibrary.wiley.com/doi/abs/10.1029/2017JA024912. 4.2.1

Golden, D. I., M. Spasojevic, and U. S. Inan, 2009. Diurnal dependence of ELF/VLF hiss and its relation to chorus at L = 2.4. *Journal of Geophysical Research: Space Physics*, **114**(A5). 10.1029/2008JA013946, URL https://agupubs.onlinelibrary.wiley.com/doi/abs/10.1029/2008JA013946. 3.2

Gou, X., L. Li, B. Zhou, Y. Zhang, L. Xie, et al., 2023. Electrostatic Ion Cyclotron Waves Observed by CSES in the Equatorial Plasma Bubble. *Geophysical Research Letters*, **50**(4), e2022GL101,791. E2022GL101791 2022GL101791, 10.1029/2022GL101791, URL https://agupubs.onlinelibrary.wiley.com/doi/abs/10.1029/2022GL101791. 4.1.2

Heacock, R. R., 1974. Whistler-like pulsation events in the frequency range 20 to 200 Hz. *Geophysical Research Letters*, **1**(2), 77–79. 10.1029/GL001i002p00077, URL https://agupubs.onlinelibrary.wiley.com/doi/abs/10.1029/GL001i002p00077. 3.7, 4.2.1

Hu, Y., Z. Zhima, T. Wang, C. Lu, D. Yang, X. Sun, T. Tang, and J. Cao, 2024. The Typical ELF/VLF Electromagnetic Wave Activities in the Upper Ionosphere Recorded by the China Seismo-Electromagnetic Satellite. *Remote Sensing*, **16**(15). 10.3390/rs16152835, URL https://www.mdpi.com/2072-4292/16/15/2835. 3.5, 4.2.4

Hulot, G., P. Coïsson, L. Chauvet, P. Vigneron, J.-M. Leger, and T. Jager, 2022. Swarm ASM burst-mode L1b data and the L2 whistler product they allow to derive. In LPS 2022 - 2022 Living Planet Symposium. ESA, ESA, Bonn, Germany. URL https://cea.hal.science/cea-04454612. 3.4

Hulot, G., P. Vigneron, J.-M. Léger, I. Fratter, N. Olsen, et al., 2015. Swarm's absolute magnetometer experimental vector mode, an innovative capability for space magnetometry. *Geophysical Research Letters*, **42**(5), 1352–1359. 10.1002/2014GL062700, URL https://agupubs.onlinelibrary.wiley.com/doi/abs/10.1002/2014GL062700. 1

Jenner, M., P. Coïsson, G. Hulot, D. Buresova, V. Truhlik, and L. Chauvet, 2024. Total Root Electron Content: A New Metric for the Ionosphere Below Low Earth Orbiting Satellites. *Geophysical Research Letters*, **51**(15), e2024GL110,559. E2024GL110559 2024GL110559, 10.1029/2024GL110559, URL https://agupubs.onlinelibrary.wiley.com/doi/abs/10.1029/2024GL110559. 1

Kim, H., M. R. Lessard, J. LaBelle, and J. R. Johnson, 2006. Narrow-band extremely low frequency (ELF) wave phenomena observed at South Pole Station. *Geophysical Research Letters*, **33**(6). 10.1029/2005GL023638, URL https://agupubs.onlinelibrary.wiley.com/doi/abs/10.1029/2005GL023638. 3.7, 4.2.1

Kim, H., K. Shiokawa, J. Park, Y. Miyoshi, Y. Miyashita, et al., 2020. Ionospheric Plasma Density Oscillation Related to EMIC Pc1 Waves. *Geophysical Research Letters*, **47**(15), e2020GL089,000. E2020GL089000 2020GL089000, 10.1029/2020GL089000, URL https://agupubs.onlinelibrary.wiley.com/doi/abs/10.1029/2020GL089000. 3.2

Knudsen, D., J. Burchill, S. Buchert, A. Eriksson, R. Gill, J.-E. Wahlund, L. Åhlén, M. Smith, and B. Moffat, 2017. Thermal ion imagers and Langmuir probes in the Swarm electric field instruments. *Journal of Geophysical Research: Space Physics*, **122**(2), 2655–2673. 10.1002/2016JA022571, URL https://agupubs.onlinelibrary.wiley.com/doi/abs/10.1002/2016JA022571. 3

Léger, J.-M., F. Bertrand, T. Jager, M. Le Prado, I. Fratter, and J.-C. Lalaurie, 2009. Swarm Absolute Scalar and Vector Magnetometer Based on Helium 4 Optical Pumping. *Procedia Chemistry*, **1**(1), 634–637. Proceedings of the Eurosensors XXIII conference, 10.1016/j.proche.2009.07.158. 1, 1

Liao, L., S. Zhao, Z. Ma, X. Shen, H. Peng, and H. Lu, 2024. An Investigation of the Third Harmonic Power Line Emission in the Topside Ionosphere During the Recent Solar Minimum Period. *Journal of Geophysical Research: Space Physics*, **129**(8), e2024JA032,899. E2024JA032899 2024JA032899, 10.1029/2024JA032899, URL https://agupubs.onlinelibrary.wiley.com/doi/abs/10.1029/2024JA032899. 3.1, 4.1.1

Léger, J.-M., T. Jager, F. Bertrand, G. Hulot, L. Brocco, P. Vigneron, X. Lalanne, A. Chulliat, and I. Fratter, 2015. In-flight performance of the Absolute Scalar Magnetometer vector mode on board the Swarm satellites. *Earth, Planets and Space*, **67**(1), 57. 10.1186/s40623-015-0231-1, URL https://doi.org/10.1186/s40623-015-0231-1. 1, 2, 3.1, 3.3

Lühr, H., and Y.-L. Zhou, 2023. Distinguishing Electromagnetic Ion Cyclotron (EMIC) Waves From Other Pc1 Signatures in Satellite Recordings by Means of the Swarm Satellite Constellation. *Journal of Geophysical Research: Space Physics*, **128**(11), e2023JA031,817. E2023JA031817 2023JA031817, 10.1029/2023JA031817, URL https://agupubs.onlinelibrary.wiley.com/doi/abs/10.1029/2023JA031817. 4.1.2

Merayo, J., J. L. Jørgensen, E. Friis-Christensen, P. Brauer, F. Primdahl, P. S. Jørgensen, T. H. Allin, and T. Denver. Small Satellites for Earth Observation, chap. The Swarm Magnetometry Package, 143–151. Springer Netherlands, 2008. ISBN 978-1-4020-6943-7. 10.1007/978-1-4020-6943-7_13, URL https://doi.org/10.1007/978-1-4020-6943-7_13. 4.2.5

Nielsen, J. B., 2021. Swarm Level 1b Product Definition. *Tech. Rep. SW-RS-DSC-SY-0007, Issue 5.26*, National Space Institute, Technical University of Denmark. Restricted: For use within the ESA Swarm project only, URL https://earth.esa.int/eogateway/documents/20142/37627/swarm-level-1b-product-definition-specification.pdf. 1

Němec, F., M. Parrot, and O. Santolík, 2015. Power line harmonic radiation observed by the DEMETER spacecraft at 50/60 Hz and low harmonics. *Journal of Geophysical Research: Space Physics*, **120**(10), 8954–8967. 10.1002/2015JA021682, URL https://agupubs.onlinelibrary.wiley.com/doi/abs/10.1002/2015JA021682. 3.1

Němec, F., O. Santolík, M. Parrot, and J. Bortnik, 2008. Power line harmonic radiation observed by satellite: Properties and propagation through the ionosphere. *Journal of Geophysical Research: Space Physics*, **113**(A8). 10.1029/2008JA013184, URL https://agupubs.onlinelibrary.wiley.com/doi/abs/10.1029/2008JA013184. 4.1.1

Park, J., M. Noja, C. Stolle, and H. Lühr, 2013. The Ionospheric Bubble Index deduced from magnetic field and plasma observations onboard Swarm. *Earth, Planets and Space*, **65**, 1333–1344. 10.5047/eps.2013.08.005, URL https://doi.org/10.5047/eps.2013.08.005. 3, 3.2

Parrot, M., F. Němec, and O. Santolík, 2014. Statistical analysis of VLF radio emissions triggered by power line harmonic radiation and observed by the low-altitude satellite DEMETER. *Journal of Geophysical Research: Space Physics*, **119**(7), 5744–5754. 10.1002/2014JA020139, URL https://insu.hal.science/insu-01174151. 4.1.1

Pfaff, R., H. Freudenreich, F. Simoes, and C. Liebrecht, 2014. Observations of 50/60 Hz power line radiation in the low latitude ionosphere detected by the electric field instrument on the C/NOFS satellite. In 2014 XXXIth URSI General Assembly and Scientific Symposium (URSI GASS), 1–1. 10.1109/URSIGASS.2014.6929584. 4.1.1

Pilipenko, V. A., M. Parrot, E. N. Fedorov, and N. G. Mazur, 2019. Electromagnetic Field in the Upper Ionosphere From ELF Ground-Based Transmitter. *Journal of Geophysical Research: Space Physics*, **124**(10), 8066–8080. 10.1029/2019JA026929, URL https://agupubs.onlinelibrary.wiley.com/doi/abs/10.1029/2019JA026929. 3.1, 4.1.1

Ritter, P., H. Lühr, and J. Rauberg, 2013. Determining field-aligned currents with the Swarm constellation mission. *Earth, Planets and Space*, **65**(11), 1285–1294. 10.5047/eps.2013.09.006, URL https://doi.org/10.5047/eps.2013.09.006. 3

Rodríguez-Zuluaga, J., C. Stolle, and J. Park, 2017. On the direction of the Poynting flux associated with equatorial plasma depletions as derived from Swarm. *Geophysical Research Letters*, **44**(12), 5884–5891. 10.1002/2017GL073385, URL https://agupubs.onlinelibrary.wiley.com/doi/abs/10.1002/2017GL073385. 3.2

Ross, J. P. J., S. A. Glauert, R. B. Horne, C. E. J. Watt, and N. P. Meredith, 2021. On the Variability of EMIC Waves and the Consequences for the Relativistic Electron Radiation Belt Population. *Journal of Geophysical Research: Space Physics*, **126**(12), e2021JA029,754. E2021JA029754 2021JA029754, 10.1029/2021JA029754, URL https://agupubs.onlinelibrary.wiley.com/doi/abs/10.1029/2021JA029754. 3.5

Santolík, O., J. Chum, M. Parrot, D. A. Gurnett, J. S. Pickett, and N. Cornilleau-Wehrlin, 2006. Propagation of whistler mode chorus to low altitudes: Spacecraft observations of structured ELF hiss. *Journal of Geophysical Research: Space Physics*, **111**(A10). 10.1029/2005JA011462, URL https://agupubs.onlinelibrary.wiley.com/doi/abs/10.1029/2005JA011462. 3.2

Sentman, D. D., and D. A. Ehring, 1994. Midlatitude detection of ELF whistlers. *Journal of Geophysical Research: Space Physics*, **99**(A2), 2183–2190. 10.1029/93JA02103, URL https://agupubs.onlinelibrary.wiley.com/doi/abs/10.1029/93JA02103. 3.7, 4.2.1

Sigsbee, K., C. A. Kletzing, J. Faden, and C. W. Smith, 2023. Occurrence Rates of Electromagnetic Ion Cyclotron (EMIC) Waves With Rising Tones in the Van Allen Probes Data Set. *Journal of Geophysical Research: Space Physics*, **128**(2), e2022JA030,548. E2022JA030548 2022JA030548, 10.1029/2022JA030548, URL https://agupubs.onlinelibrary.wiley.com/doi/abs/10.1029/2022JA030548. 3.5

Smith, A. R. A., M. Pačes, and D. Santillan, 2022. ESA-VirES/VirES-Python-Client (v0.11.1). *Zenodo*. 10.5281/zenodo.7271900, URL https://doi.org/10.5281/zenodo.4476534. 3

Song, S., F. Yin, Q. Yan, H. Lühr, C. Xiong, Y. Jiang, and P. Liu, 2025. Comprehensive analysis of noise in Macau Science Satellite-1 vector magnetometer data. *Earth and Planetary Physics*, **9**(3), 532–540. 10.26464/epp2025031, URL https://www.eppcgs.org/en/article/doi/10.26464/epp2025031. 4.2.5

Spogli, L., L. Alfonsi, and C. Cesaroni, 2023. Stepping Into an Equatorial Plasma Bubble With a Swarm Overfly. *Space Weather*, **21**(5), e2022SW003,331. 10.1029/2022SW003331, URL https://agupubs.onlinelibrary.wiley.com/doi/abs/10.1029/2022SW003331. 3.2

Vigneron, P., G. Hulot, J.-M. Léger, and T. Jager, 2021. Using improved Swarm's experimental absolute vector mode data to produce a candidate Definitive Geomagnetic Reference Field (DGRF) 2015.0 model. *Earth, Planets and Space*, **73**(1), 197. 10.1186/s40623-021-01529-7, URL https://doi.org/10.1186/s40623-021-01529-7. 1

Vigneron, P., G. Hulot, N. Olsen, J.-M. Léger, T. Jager, L. Brocco, O. Sirol, P. Coïsson, X. Lalanne, and A. Chulliat, 2015. A 2015 International Geomagnetic Reference Field (IGRF) candidate model based on Swarm's experimental absolute magnetometer vector mode data. *Earth, Planets and space*, **67**, 95. 10.1186/s40623-015-0265-4, URL https://doi.org/10.1186/s40623-015-0265-4. 1

Wang, H., Y. He, and H. Lühr, 2022. Analysis of Ionospheric Compressional Waves and Electron Density Oscillation During Storm Periods Using Swarm Observations. *Journal of Geophysical Research: Space Physics*, **127**(8), e2022JA030,409. E2022JA030409 2022JA030409, 10.1029/2022JA030409, URL https://agupubs.onlinelibrary.wiley.com/doi/abs/10.1029/2022JA030409. 3.5

Wang, Y.-C., K. Wang, H.-T. Su, and R.-R. Hsu, 2005. Low-latitude ELF-whistlers observed in Taiwan. *Geophysical Research Letters*, **32**(8). 10.1029/2005GL022412, URL https://agupubs.onlinelibrary.wiley.com/doi/abs/10.1029/2005GL022412. 3.7, 4.2.1

Xia, Z., L. Chen, Z. Zhima, O. Santolík, R. B. Horne, and M. Parrot, 2019. Statistical Characteristics of Ionospheric Hiss Waves. *Geophysical Research Letters*, **46**(13), 7147–7156. 10.1029/2019GL083275, URL https://agupubs.onlinelibrary.wiley.com/doi/abs/10.1029/2019GL083275. 3.5, 4.2.3

Yin, F., H. Lühr, J. Park, J. Rauberg, and I. Michaelis, 2015. Noise features of the CHAMP vector magnetometer in the 1–25Hz frequency range. *Sensors and Actuators A: Physical*, **222**, 272–283. 10.1016/j.sna.2014.12.024, URL https://www.sciencedirect.com/science/article/pii/S0924424714005469. 4.2.5

Zhao, S., L. Liao, X. Shen, H. Lu, Z. Zhima, J. Huang, and C. Zhou, 2022. CSES Satellite Observations of 50 Hz Power Line Radiation Over Mainland China and Its Response to COVID-19. *Journal of Geophysical Research: Space Physics*, **127**(9), e2022JA030,693. 10.1029/2022JA030693, URL https://agupubs.onlinelibrary.wiley.com/doi/abs/10.1029/2022JA030693. 3.1, 4.1.1

Zhima, Z., L. Chen, Y. Xiong, J. Cao, and H. Fu, 2017. On the Origin of Ionospheric Hiss: A Conjugate Observation. *Journal of Geophysical Research: Space Physics*, **122**(11), 11,784–11,793. 10.1002/2017JA024803, URL https://agupubs.onlinelibrary.wiley.com/doi/abs/10.1002/2017JA024803. 3.5, 4.2.3

Zhima, Z., J. Huang, X. Shen, Z. Xia, L. Chen, et al., 2020. Simultaneous Observations of ELF/VLF Rising-Tone Quasiperiodic Waves and Energetic Electron Precipitations in the High-Latitude Upper Ionosphere. *Journal of Geophysical Research: Space Physics*, **125**(5), e2019JA027,574. E2019JA027574 2019JA027574, 10.1029/2019JA027574, URL https://agupubs.onlinelibrary.wiley.com/doi/abs/10.1029/2019JA027574. 4.2.4